



1 **Impact of dust addition on the metabolism of Mediterranean**
2 **plankton communities and carbon export under present and**
3 **future conditions of pH and temperature**

4 Frédéric Gazeau¹, France Van Wambeke², Emilio Marañón³, María Pérez-Lorenzo³, Samir
5 Alliouane¹, Christian Stolpe¹, Thierry Blasco¹, Nathalie Leblond⁴, Birthe Zäncker^{5,6}, Anja
6 Engel⁶, Barbara Marie⁷, Julie Dinasquet^{7,8}, Cécile Guieu¹

7 ¹ Sorbonne Université, CNRS, Laboratoire d'Océanographie de Villefranche, LOV, 06230
8 Villefranche-sur-Mer, France

9 ² Aix-Marseille Université, Université de Toulon, CNRS/INSU, IRD, Mediterranean Institute of
10 Oceanography (MIO), UM 110, 13288, Marseille, France

11 ³ Department of Ecology and Animal Biology, Universidade de Vigo, 36310 Vigo, Spain

12 ⁴ Sorbonne Université, CNRS, Institut de la Mer de Villefranche, IMEV, 06230 Villefranche-sur-
13 Mer, France

14 ⁵ The Marine Biological Association of the UK, PL1 2PB Plymouth, United Kingdom

15 ⁶ GEOMAR Helmholtz Centre for Ocean Research, Kiel, Germany

16 ⁷ CNRS, Sorbonne Université, Laboratoire d'Océanographie Microbienne, LOMIC, F-66650
17 Banyuls-sur-Mer, France

18 ⁸ Scripps Institution of Oceanography, University of California San Diego, USA

19 Correspondence to: Frédéric Gazeau (f.gazeau@obs-vlfr.fr)

20 Keywords: Mediterranean Sea; Atmospheric deposition; Plankton community metabolism;

21 Carbon export; Ocean acidification; Ocean warming



22

23 **Abstract**

24 Although atmospheric dust fluxes from arid as well as human-impacted areas represent a
25 significant source of nutrients to surface waters of the Mediterranean Sea, studies focusing on the
26 evolution of the metabolic balance of the plankton community following a dust deposition event
27 are scarce and none were conducted in the context of projected future levels of temperature and
28 pH. Moreover, most of the experiments took place in coastal areas. In the framework of the
29 PEACETIME project, three dust-addition perturbation experiments were conducted in 300-L
30 tanks filled with surface seawater collected in the Tyrrhenian Sea (TYR), Ionian Sea (ION) and
31 in the Algerian basin (FAST) onboard the R/V “Pourquoi Pas?” in late spring 2017. For each
32 experiment, six tanks were used to follow the evolution of chemical and biological stocks,
33 biological activity and particle export. The impacts of a dust deposition event simulated at their
34 surface were followed under present environmental conditions and under a realistic climate
35 change scenario for 2100 (ca. + 3 °C and -0.3 pH units). The tested waters were all typical of
36 stratified oligotrophic conditions encountered in the open Mediterranean Sea at this period of the
37 year, with low rates of primary production and a metabolic balance towards net heterotrophy.
38 The release of nutrients after dust seeding had very contrasting impacts on the metabolism of the
39 communities, depending on the station investigated. At TYR, the release of new nutrients was
40 followed by a negative impact on both particulate and dissolved ¹⁴C-based production rates,
41 while heterotrophic bacterial production strongly increased, driving the community to an even
42 more heterotrophic state. At ION and FAST, the efficiency of organic matter export due to
43 mineral/organic aggregation processes was lower than at TYR likely related to a lower
44 quantity/age of dissolved organic matter present at the time of the seeding. At these stations, both



45 the autotrophic and heterotrophic community benefited from dust addition, with a stronger
46 relative increase in autotrophic processes observed at FAST. Our study showed that the potential
47 positive impact of dust deposition on primary production depends on the initial composition and
48 metabolic state of the investigated community. This potential is constrained by the quantity of
49 nutrients added in order to sustain both the fast response of heterotrophic prokaryotes and the
50 delayed one of primary producers. Finally, under future environmental conditions, heterotrophic
51 metabolism was overall more impacted than primary production, with the consequence that all
52 integrated net community production rates decreased with no detectable impact on carbon
53 export, therefore reducing the capacity of surface waters to sequester anthropogenic CO₂.



54

55 **1. Introduction**

56 Low Nutrient Low Chlorophyll (LNLC) areas represent 60% of the global ocean surface
57 area (Longhurst et al., 1995) and, although phytoplankton production there is limited by the
58 availability of nitrogen, phosphorus and iron, it accounts for 50% of global carbon export
59 (Emerson et al., 1997). Atmospheric dust fluxes from arid as well as anthropogenic sources
60 represent a significant source of these nutrients to surface waters in these regions and as such
61 could play a significant role in stimulating primary production (e.g. Bishop et al., 2002; Guieu et
62 al., 2014b; Jickells and Moore, 2015), potentially increasing the efficiency of the biological
63 pump in the sequestration of atmospheric CO₂. However, as heterotrophic prokaryotes have been
64 shown to outcompete phytoplankton during nutrient addition experiments (e.g. Guieu et al.,
65 2014a; Mills et al., 2008; Thingstad et al., 2005), dust deposition could induce even stronger
66 enhancements of heterotrophic bacterial production and/or respiration rates thereby reducing net
67 atmospheric CO₂ drawdown and the potential for carbon export outside the euphotic zone (Guieu
68 et al., 2014b). Indeed, several experiments conducted in the Atlantic Ocean and in the
69 Mediterranean Sea have shown a fast and dominant effect of dust additions on heterotrophic
70 bacterioplankton metabolism (Herut et al., 2005, 2016; Lekunberri et al., 2010; Marañón et al.,
71 2010; Pulido-Villena et al., 2008, 2014). However, to the best of our knowledge, no study
72 focused on the evolution of the metabolic balance of the plankton community after such a dust
73 event in the open sea. The metabolic balance (or net community production, NCP) is defined as
74 the difference between gross primary production (GPP) of autotrophic organisms and community



75 respiration (CR) of both autotrophic and heterotrophic organisms, revealing the capacity of a
76 system to sequester carbon via the biological pump.

77 The Mediterranean Sea is a perfect example of LNLC regions and receives anthropogenic
78 aerosols originating from industrial and domestic activities from all around the basin and other
79 parts of Europe and pulses of natural inputs from the Sahara (e.g. Bergametti et al., 1989;
80 Desboeufs et al., 2018). These atmospheric depositions, mostly in the form of pulsed inputs
81 (Loÿe-Pilot and Martin, 1996), provide new nutrients (Guieu et al., 2010; Kouvarakis et al.,
82 2001; Markaki et al., 2003; Ridame and Guieu, 2002) to the surface waters with fluxes that are of
83 the same order of magnitude as riverine inputs (Powley et al., 2017). These significant nutrient
84 enrichments likely support primary production especially during the stratification period (Bonnet
85 et al., 2005; Ridame and Guieu, 2002), however no clear correlation between dust and ocean
86 color have been evidenced from long series of satellite observations (Guieu and Ridame, 2020).
87 This raises the question on which compartment (autotrophic or heterotrophic) benefits the most
88 from these transient relieves in nutrient limitation.

89 In response to ocean warming and increased stratification, LNLC areas are expected to
90 expand in the future (Irwin and Oliver, 2009; Polovina et al., 2008) due to lower nutrient supply
91 from sub-surface waters (Behrenfeld et al., 2006). Furthermore, dust deposition could increase in
92 the future due to desertification (Moulin and Chiapello, 2006), although so far the trend for
93 deposition remains uncertain because the drying of the Mediterranean basin might also induce
94 less wet deposition over the basin (Laurent et al., 2021). Nevertheless, whether the fluxes
95 increase or not in the coming decades and centuries, new nutrients from atmospheric sources will
96 play an important role in a surface mixed layer even more stratified and isolated from the deeper
97 nutrient-rich layer. The question remains on how plankton metabolism and carbon export would



98 respond in a warmer and more acidified ocean. Indeed, with an average annual anthropogenic
99 CO₂ uptake, during the period 2010 to 2019, of 2.5 ± 0.6 GtC (~22.9% of anthropogenic
100 emissions; Friedlingstein et al., 2020), the oceans substantially contribute towards slowing down
101 the increase in atmospheric CO₂ concentrations, and therefore towards limiting terrestrial and
102 ocean warming. However, this massive CO₂ input induces global changes in seawater chemistry
103 referred to as “ocean acidification” because increased CO₂ concentration lowers seawater pH
104 (i.e. increases its acidity).

105 Although the response of plankton metabolism to ocean warming has been shown to be
106 highly dependent on resource availability (Lewandowska et al., 2014), both for heterotrophic
107 bacteria (Lopez-Urrutia and Moran, 2007) and phytoplankton (Marañón et al., 2018), it has been
108 suggested that ocean warming will substantially weaken the ocean CO₂ sink in the future as a
109 consequence of stronger increase in remineralization than in photosynthesis processes, following
110 the metabolic theory of ecology (MTE; Brown et al., 2004; Gillooly et al., 2001). Ocean
111 acidification alone has been shown to exert no or very limited influence on plankton metabolism
112 in the Mediterranean Sea (Maugendre et al., 2017a; Mercado et al., 2014). To the best of our
113 knowledge, only Maugendre et al. (2015) studied the combined impact of ocean warming and
114 acidification on plankton metabolism in the Mediterranean Sea. They found a very limited
115 impact of ocean acidification on the plankton community and a positive impact of warming on
116 small phytoplankton species (e.g. Cyanobacteria) with a potential decrease of the export and
117 energy transfer to higher trophic levels. Nevertheless, that study was conducted under nutrient
118 depleted conditions and there is still a need to assess the combined impact of warming and
119 acidification on the metabolic balance of plankton communities in this region, following a
120 transient relief in nutrient availability (Maugendre et al., 2017b).



121 So far there has been no attempt to evaluate the evolution of plankton metabolism and
122 carbon export following atmospheric deposition in the context of future levels of temperature
123 and pH. Such experiments were conducted in the frame of the PEACETIME project (ProcEss
124 studies at the Air-sEa Interface after dust deposition in the MEditerranean sea; [http://peacetime-](http://peacetime-project.org/)
125 [project.org/](http://peacetime-project.org/)) during the cruise on board the R/V “Pourquoi Pas?” in May/June 2017 (Guieu et al.,
126 2020). The project aimed at extensively studying and parameterizing the chain of processes
127 occurring in the Mediterranean Sea after atmospheric deposition, especially of Saharan dust, and
128 to put them in perspective of on-going environmental changes. During this cruise, three
129 perturbation experiments were conducted in 300-L tanks filled with surface seawater collected in
130 the Tyrrhenian Sea (TYR), Ionian Sea (ION) and in the Algerian basin (FAST; Fig. 1). Six tanks
131 were used to follow the evolution of chemical and biological stocks, biological activity and
132 export, following a wet dust deposition event simulated at their surface, both under present
133 environmental conditions and following a realistic climate change scenario for 2100 (ca. + 3 °C
134 and -0.3 pH units; IPCC, 2013). A companion paper presents the general setup of the
135 experiments and the impacts of dust under present and future environmental conditions on
136 nutrients and biological stocks (Gazeau et al., 2020). Here, we focus on the impacts of dust
137 seeding on plankton metabolism (e.g. primary production, heterotrophic prokaryote production)
138 and carbon export.



139

140 **2. Material and Methods**

141 **2.1. General set-up**

142 The general set-up of the experiments is fully detailed in Gazeau et al. (2020). Briefly,
143 three experiments were performed at the long duration stations TYR, ION and FAST during the
144 Peacetime cruise onboard R/V “Le Pourquoi Pas?” (Fig. 1). During these experiments (3 to 4
145 days each), seawater was incubated in 300-L tanks (Fig. S1) installed in a temperature-controlled
146 container, in which the irradiance spectrum and intensity can be finely controlled and in which
147 future ocean acidification and warming conditions can be fully reproduced. The tanks were made
148 of high-density polyethylene (HDPE) and were trace-metal free in order to avoid contaminations,
149 with a height of 1.09 m, a diameter of 0.68 m, a surface area of 0.36 m² and a volume of 0.28 m³.
150 The conical base of the tanks was equipped with a sediment trap that was left open during the
151 duration of the experiments and removed at the end. The experimental protocol comprised two
152 unmodified control tanks (C1 and C2), two tanks enriched with Saharan dust (D1 and D2) and
153 two tanks enriched with Saharan dust and maintained simultaneously under warmer (+ 3 °C) and
154 acidified (-0.3 pH unit) conditions (G1 and G2). At the three stations, tanks were always filled at
155 the end of the day before the start of the experiments: TYR (17/05/2017), ION (25/05/2017) and
156 FAST (02/06/2017). The tanks were filled by means of a large peristaltic pump (Verder© VF40
157 with EPDM hose, flow of 1200 L h⁻¹) collecting seawater below the base of the boat (depth of ~
158 5 m), used to supply continuously surface seawater to a series of instruments during the entire
159 campaign. While filling the tanks, seawater was sampled for the measurements of selected
160 parameters (sampling time = t-12h). After filling the tanks, seawater was slowly warmed



161 overnight using 500 W heaters, controlled by temperature-regulation units (COREMA©), in G1
162 and G2 to reach an offset of + 3 °C. ¹³C-bicarbonate was added to all tanks at 4:00 am (all times
163 in local time) and G1 and G2 were acidified by addition of CO₂-saturated filtered (0.2 µm)
164 seawater (~1.5 L in 300 L; collected when filling the tanks at each station) at 4:30 am to reach a
165 pH offset of -0.3. Sampling for many parameters took place prior to dust seeding (sampling time
166 = t₀). Dust seeding was performed between 7:00 and 9:00 in tanks D1, D2, G1 and G2. The same
167 dust analog was used and the same dust flux was simulated as for the DUNE 2009 experiments
168 described in Desboeufs et al. (2014). To mimic a realistic wet flux event of 10 g m⁻², 3.6 g of this
169 analog dust were quickly diluted into 2 L of ultrahigh-purity water (UHP water; 18.2 MΩ cm⁻¹
170 resistivity), and sprayed at the surface of the tanks using an all-plastic garden sprayer (duration =
171 30 min). Depending on the considered parameter or process, seawater sampling was conducted 1
172 h (t_{1h}), 6 h (t_{6h}), 12 h (t_{12h}), 24 h (t_{24h}), 48 h (t_{48h}) and 72 h (t_{72h}) (+ 96 h = t_{96h} for station
173 FAST) after dust addition. Acid-washed silicone tubes were used for transferring the water
174 collected from the tanks to the different vials or containers.

175 **2.2. Stocks**

176 **2.2.1. Dissolved and particulate organic carbon**

177 The concentration of dissolved organic carbon (DOC) was determined from duplicate 10
178 mL GF/F (pre-combusted, Whatman) filtered subsamples that were transferred to pre-combusted
179 glass ampoules, acidified with H₃PO₄ (final pH = 2) and sealed. The sealed glass ampoules were
180 stored in the dark at room temperature until analysis at the Laboratoire d'Océanographie
181 Microbienne (LOMIC). DOC measurements were performed on a Shimadzu© TOC-V-CSH



182 (Benner and Strom, 1993). Prior to injection, DOC samples were sparged with CO₂-free air for 6
183 min to remove inorganic carbon. Sample (100 µL) were injected in triplicate and the analytical
184 precision was 2%. Standards were prepared with acetanilid.

185 Seawater samples for measurements of particulate organic carbon concentrations (POC; 2
186 L) were taken at t-12h, t₀, t_{12h}, t_{24h}, t_{48h} and t_{72h} (or t_{96h} for station FAST), filtered on pre-
187 combusted GF/F membranes, dried at 60 °C and analyzed at the Laboratoire d'Océanographie de
188 Villefranche (LOV, France) following decarbonation with a drop of HCl 2N, on an elemental
189 analyzer coupled with an isotope ratio mass spectrometer (EA-IRMS; Vario Pyrocube-Isoprime
190 100, Elementar©).

191 **2.2.2. Total hydrolysable carbohydrates and amino acids**

192 For total hydrolysable carbohydrates and amino acids, samples were taken at t₀, t_{6h},
193 t_{24h}, t_{48h} and t_{72h} at all stations. For total hydrolysable carbohydrates (TCHO) > 1 kDa,
194 samples (20 mL) were filled into pre-combusted glass vials (8 h, 500 °C) and stored at -20 °C
195 pending analysis. Prior to analysis, samples were desalted with membrane dialysis (1 kDa
196 MWCO, Spectra Por) at 1 °C for 5 h. Samples were subsequently hydrolyzed for 20 h at 100 °C
197 with 0.8 M HCl final concentration followed by neutralization using acid evaporation (N₂, for 5
198 h at 50 °C). TCHO were analysed at GEOMAR using high performance anion exchange
199 chromatography with pulsed amperometric detection (HPAEC-PAD), on a Dionex ICS 3000 ion
200 chromatography system following the procedure of Engel and Händel (2011). Two replicates per
201 TCHO sample were analyzed.

202 For total hydrolysable amino acids (TAA), samples (5 mL) were filled into pre-
203 combusted glass vials (8 h, 500 °C) and stored at -20 °C. Samples were hydrolyzed at 100 °C for



204 20 h with 1 mL 30% HCl (Suprapur®, Merck) added to 1 mL of sample, and neutralized by acid
205 evaporation under vacuum at 60 °C in a microwave. Samples were analyzed by high
206 performance liquid chromatography (HPLC) using an Agilent 1260 HPLC system following a
207 modified version of established methods (Dittmar et al., 2009; Lindroth and Mopper, 1979).
208 Separation of 13 amino acids with a C18 column (Phenomenex Kinetex, 2.6 µm, 150 x 4.6 mm)
209 was obtained after in-line derivatization with o-phthaldialdehyde and mercaptoethanol. A
210 gradient with solvent A containing 5 % acetonitrile (LiChrosolv, Merck, HPLC gradient grade)
211 in sodium dihydrogenphosphate (Suprapur®, Merck) buffer (pH 7.0) and solvent B being
212 acetonitrile was used for analysis. A gradient from 100% solvent A to 78% solvent A was
213 produced in 50 min. Two replicates per TAA sample were analyzed.

214 **2.2.3. Transparent exopolymer particles**

215 Samples for transparent exopolymer particles (TEP) were taken at t₀, t_{24h} and t_{72h} at all
216 stations. The abundance and area of TEP were microscopically measured following the
217 procedure given in Engel (2009). Samples of 10-50 mL were directly filtered under low vacuum
218 (< 200 mbar) onto a 0.4 µm Nucleopore membrane (Whatman©) filter, stained with 1 mL Alcian
219 Blue solution (0.2 g l⁻¹ w/v) for 3 s and rinsed with MilliQ water. Filters were mounted on
220 Cytoclear© slides and stored at -20 °C until analysis. Two filters per sample with 30 images each
221 were analyzed using a Zeiss Axio Scope.A1 (Zeiss©) and an AxioCam MRc (Zeiss©). The
222 pictures with a resolution of 1388 x 1040 pixels were saved using AxioVision LE64 Rel. 4.8
223 (Zeiss©). All particles larger than 0.2 µm² were analyzed. ImageJ© and R were subsequently
224 used for image analysis (Schneider, Rasband and Eliceiri 2012, R Core Team, 2014). Filters
225 prepared with 10 mL MilliQ water instead of samples served as a blank. The carbon content of
226 TEP (TEP-C) was estimated after Mari (1999) using the size-dependent relationship:



$$227 \quad TEP-C = a \sum_i n_i r_i^D \quad (1)$$

228 with n_i being the number of TEP in the size class i and r_i being the mean equivalent spherical
229 radius of the size class. The constant $a = 0.25 * 10^{-6}$ ($\mu\text{g C}$) and the fractal dimension of
230 aggregates $D = 2.55$ were used as proposed by Mari (1999). To relate to organic carbon
231 concentration in seawater, data for TEP-C are given as $\mu\text{mol L}^{-1}$.

232 **2.3. Processes**

233 **2.3.1. Dissolved and particulate ^{14}C incorporation rates**

234 The photosynthetic production of particulate ($< 0.2\text{-}2 \mu\text{m}$ and $> 2 \mu\text{m}$ size fractions) and
235 dissolved organic matter was determined from samples taken at t_0 , $t_{24\text{h}}$, $t_{48\text{h}}$ and $t_{72\text{h}}$ (or $t_{96\text{h}}$
236 at station FAST) with the ^{14}C -uptake technique. From each tank, four polystyrene bottles (70
237 mL; three light and one dark bottles) were filled with sampled seawater and amended with 40
238 μCi of $\text{NaH}^{14}\text{CO}_3$. Bottles were incubated for 8 h in two extra 300 L tanks maintained under
239 similar light and temperature regimes than in the experimental tanks (ambient temperature for
240 C1, C2, D1 and D2 and ambient temperature + 3 °C for G1 and G2). Incubations were
241 terminated by sequential filtration of the sample through polycarbonate filters (pore sizes 2 μm
242 and 0.2 μm , 47 mm diameter) using low-pressure vacuum. Filters were exposed for 12 h to
243 concentrated HCl fumes to remove non-fixed, inorganic ^{14}C , and then transferred to 4 mL plastic
244 scintillation vials to which 3.5 mL of scintillation cocktail (Ultima Gold XR, Perkin Elmer©)
245 were added. For the measurement of dissolved primary production, a 5 mL aliquot of each
246 sampling bottle was filtered, at the end of incubation, through a 0.2 μm polycarbonate filter (25
247 mm diameter). This filtration was conducted, under low-pressure vacuum, in a circular filtration



248 manifold that allows the recovery of the filtrate into 20 mL scintillation vials. The filtrates were
249 acidified with 200 μL of 50% HCl and maintained in an orbital shaker for 12 h. Finally, 15 mL
250 of liquid scintillation cocktail was added to each sample. All filter and filtrate samples were
251 measured onboard in a liquid scintillation counter (Packard© 1600 TR). ^{14}C -based production
252 rates (PP; in $\mu\text{g C L}^{-1} \text{ h}^{-1}$) were calculated as:

$$253 \quad \text{PP} = C_{\text{T}} \times \left(\frac{\text{DPM}_{\text{sample}} - \text{DPM}_{\text{dark}}}{\text{DPM}_{\text{added}} \times t} \right) \quad (2)$$

254 where C_{T} is the concentration of total dissolved inorganic carbon ($\mu\text{g C L}^{-1}$), $\text{DPM}_{\text{sample}}$ and
255 DPM_{dark} are the radioactivity counts in the light and dark bottle, respectively, $\text{DPM}_{\text{added}}$ is the
256 radioactivity added to each sample, and t is the incubation time (h).

257 The percentage extracellular release (PER%) was calculated as:

$$258 \quad \text{PER}\% = \frac{\text{PPd}}{\text{PPd} + \text{PPp}} \times 100 \quad (3)$$

259 where PPd refers to ^{14}C -based dissolved production and PPp refers to ^{14}C -based particulate
260 production (sum of < 2 and > 2 μm size fractions).

261 **2.3.2. Integrated ^{13}C incorporation**

262 Addition of ^{13}C -bicarbonate ($\text{NaH}^{13}\text{CO}_3$ 99%; Sigma-Aldrich©) was performed in each
263 tank before t_0 in order to increase the isotopic level ($\delta^{13}\text{C}$ signature) of the dissolved inorganic
264 carbon pool to ca. 350‰. We followed with time the evolution of the $\delta^{13}\text{C}$ signature in dissolved
265 inorganic carbon ($\delta^{13}\text{C}-C_{\text{T}}$), dissolved organic carbon ($\delta^{13}\text{C}-\text{DOC}$) and particulate organic carbon
266 pools ($\delta^{13}\text{C}-\text{POC}$). For the analysis of the actual $\delta^{13}\text{C}-C_{\text{T}}$, 60 mL of sampled seawater (at $t-12\text{h}$,
267 t_0 , $t_{12\text{h}}$, $t_{24\text{h}}$, $t_{48\text{h}}$ and $t_{72\text{h}}$; + $t_{96\text{h}}$ at station FAST) was gently transferred to glass vials



268 avoiding bubbles. Vials were sealed after being poisoned with 12 μL saturated HgCl_2 and stored
269 upside-down at room temperature in the dark pending analysis. At the University of Leuven, a
270 helium headspace (5 mL) was created in the vials and samples were acidified with 2 mL of
271 phosphoric acid (H_3PO_4 , 99%). Samples were left to equilibrate overnight to transfer all C_T to
272 gaseous CO_2 . Samples were injected in the carrier gas stream of an EA-IRMS (Thermo©
273 EA1110 and Delta V Advantage), and data were calibrated with NBS-19 and LSVEC standards
274 (Gillikin and Bouillon, 2007).

275 At the same frequency than for $\delta^{13}\text{C}-\text{C}_T$, samples for $\delta^{13}\text{C}-\text{DOC}$ were filtered online (see
276 above), transferred to 40 mL pre-cleaned borosilicate amber EPA vials with septa caps (PTFE-
277 lined silicone) and stored in the dark pending analysis at the Ján Veizer Stable Isotope
278 Laboratory (Ottawa, Canada).

279 At t-12h, t0, t12h, t24h, t48h and t72h (or t96h at station FAST), the $\delta^{13}\text{C}-\text{POC}$ was
280 obtained based on the same measurements as described above for POC, on a an elemental
281 analyzer coupled with an isotope ratio mass spectrometer (EA-IRMS; Vario Pyrocube-Isoprime
282 100, Elementar©).

283 Carbon isotope data are expressed in the delta notation (δ) relative to Vienna Pee Dee
284 Belemnite (VPDB) standard. The carbon isotope ratio was calculated as:

$$285 \quad R_{\text{sample}} = \left(\frac{\delta^{13}\text{C}_{\text{sample}}}{1000} + 1 \right) \times R_{\text{VPDB}} \quad (4)$$

286 with $R_{\text{VPDB}} = 0.011237$.



287 **2.3.2. Community metabolism (oxygen light-dark method)**

288 At the same frequency as for ^{14}C incorporation, from each tank, a volume of 2 L was
289 sampled in plastic bottles and distributed in 15 biological oxygen demand (BOD; 60 mL)
290 borosilicate bottles. Five BOD bottles were immediately fixed with Winkler reagents (initial O_2
291 concentrations), five BOD bottles were incubated in the dark for the measurement of community
292 respiration (CR) in two incubators maintained respectively at ambient temperature for C1, C2,
293 D1 and D2 and at ambient temperature + 3 °C for G1 and G2. Additionally, five BOD bottles
294 were incubated for the measurement of net community production (NCP) in the same tanks as
295 described above for ^{14}C -incorporation. Upon completion of the incubations (24 h), samples were
296 fixed with Winkler reagents. Within one day, O_2 concentrations were measured using an
297 automated Winkler titration technique with potentiometric endpoint detection. Analyses were
298 performed on board with a Metrohm© Titrand 888 and a redox electrode (Metrohm© Au
299 electrode). Reagents and standardizations were similar to those described by Knap et al. (1996).
300 NCP and CR were estimated by regressing O_2 values against time, and CR was expressed as
301 negative values. Gross primary production (GPP) was calculated as the difference between NCP
302 and CR. The combined standard errors were calculated as:

$$303 \quad \text{SE}_{xy} = \sqrt{\text{SE}_x^2 + \text{SE}_y^2} \quad (5)$$



304 **2.3.4. Heterotrophic prokaryotic production and** 305 **ectoenzymatic activities**

306 At all sampling times, heterotrophic bacterial production (BP, *sensus stricto* referring
307 to heterotrophic prokaryotic production) was determined onboard using the microcentrifuge
308 method with the ³H- leucine (³H-Leu) incorporation technique to measure protein production
309 (Smith and Azam, 1992). The detailed protocol is in Van Wambeke et al. (2020b). Briefly,
310 triplicate 1.5 mL samples and one blank were incubated in the dark for 1-2 h in two
311 thermostated incubators maintained respectively at ambient temperature for C1, C2, D1 and
312 D2 and at ambient temperature +3 °C for G1 and G2. Incubations were ended by the addition
313 of TCA to a final concentration of 5%, followed by three runs of centrifugation at 16000 g
314 for 10 min. Pellets were rinsed with TCA 5% and ethanol 80%. A factor of 1.5 kg C mol
315 leucine⁻¹ was used to convert the incorporation of leucine to carbon equivalents, assuming no
316 isotopic dilution (Kirchman et al., 1993).

317 Ectoenzymatic activities were measured fluorometrically, using fluorogenic model
318 substrates that were L-leucine-7-amido-4-methyl-coumarin (Leu-MCA) and 4
319 methylumbelliferyl – phosphate (MUF-P) to track aminopeptidase activity (LAP) and
320 alkaline phosphatase activity (AP), respectively (Hoppe, 1983). Stocks solutions (5mM)
321 were prepared in methycellosolve and stored at -20 °C. Release of the products of LAP and
322 AP activities, MCA and MUF, were followed by measuring increase of fluorescence (exc/em
323 380/440 nm for MCA and 365/450 nm for MUF, wavelength width 5 nm) in a
324 VARIOSCAN LUXmicroplate reader calibrated with standards of MCA and MUF solutions.
325 For measurements, 2 mL of unfiltered samples from the tanks were supplemented with 100



326 μL of a fluorogenic substrate solution diluted so that different concentrations were
327 dispatched in a black 24-well polystyrene plate in duplicate (0.025, 0.05, 0.1, 0.25, 0.5, 1 μM
328 for MUF-P, 0.5, 1, 5, 10, 25 μM for MCA-leu). Incubations were carried out in the same
329 thermostatically controlled incubators than those used for BP and reproducing temperature
330 levels in the experimental tanks. Incubations lasted up to 12 h long with a reading of
331 fluorescence every 1 to 2 h, depending on the intended activities. The rate was calculated
332 from the linear part of the fluorescence versus time relationship. Boiled-water blanks were
333 run to check for abiotic activity. From varying velocities obtained, we determined the
334 parameters V_m (maximum hydrolysis velocity) and K_m (Michaelis-Menten constant which
335 reflects enzyme affinity for the substrate) by fitting the data using a non-linear regression on
336 the following equation:

$$337 \quad V = V_m \times \frac{S}{K_m + S} \quad (6)$$

338 where V is the hydrolysis rate and S the fluorogenic substrate concentration added.

339 **2.3.5. Inorganic and organic material export**

340 At the end of each experiment ($t_{72\text{h}}$ for TYR and ION and $t_{96\text{h}}$ for FAST, after artificial
341 dust seeding), the sediment traps were removed, closed and stored with formaldehyde 4%. Back
342 in the laboratory, after the swimmers were removed, the samples were rinsed to remove the salts
343 and then freeze-dried. The total amount of material collected was first weighted to measure the
344 total exported flux. Several aliquots were then weighted to measure the following components:
345 total carbon and organic carbon, lithogenic and biogenic silicates and calcium. Total carbon was
346 measured on an elemental analyzer coupled with an isotope ratio mass spectrometer (EA-IRMS;



347 Vario Pyrocube-Isoprime 100, Elementar©). Particulate organic carbon (POC) was measured in
348 the same way after removing inorganic carbon by acidification with HCl 2N. Particulate
349 inorganic carbon (PIC) was obtained by subtracting particulate organic carbon from particulate
350 total carbon. Calcium concentrations were measured by ICP-OES (Inductively Coupled Plasma -
351 Optic Emission Spectrometry; Perkin-Elmer© Optima 8000) on acid digested samples (the
352 organic matrix was removed by HNO₃ while the mineral aluminosilicate matrix was eliminated
353 with HF). Biogenic silica (BSi) and Lithogenic silica (LSi) were measured by colorimetry
354 (Analytikjena© Specor 250 plus spectrophotometer) after a NaOH/HF digestion, respectively
355 (Mosseri et al., 2005). The carbonate fraction of the exported material was determined from
356 particulate calcium concentrations (%CaCO₃ = 5/2 x (%Ca). The organic matter fraction was
357 calculated as 2 x (%POC). The lithogenic fraction was calculated as [total mass – (organic matter
358 + CaCO₃ + opal) and was very comparable to the lithogenic fraction calculated from LSi (taking
359 Si concentration in dust analog used for seeding from Desboeufs et al., 2014; ca. 11.9%). In the
360 controls, the amount of material exported was low and the entire content of the traps was filtered
361 in order to measure total mass and organic matter mass fluxes.

362

363 **2.4. Data processing**

364 All metabolic rates were integrated over the duration of the experiments using trapezoidal
365 integrations and the relative changes (in %) in tanks D and G as compared to the controls
366 (average between C1 and C2) were computed following:

$$367 \text{ Relative change} = \left(\frac{\text{Rate}_{\text{Treatment}} - \text{Rate}_{\text{Controls}}}{\text{Rate}_{\text{Controls}}} \right) \times 100 \quad (7)$$

368 Where Rate_{Treatment} is the integrated rate measured in treatments D and G (D1, D2, G1 or G2) and
369 Rate_{Controls} is the averaged integrated rates between the duplicate controls (treatment C). Daily



370 rates of ^{14}C -based production were computed from hourly rates assuming a 14 h daylight period.
371 As incubations performed from samples taken at t_0 (before dust addition) do not represent what
372 happened in the tanks between t_0 and $t_{24\text{h}}$, as a first assumption, we considered a linear
373 evolution between these rates and those measured from samples at $t_{24\text{h}}$, and recomputed an
374 average value for the time interval $t_0 - t_{24\text{h}}$. At FAST, no incubations were performed for ^{14}C
375 incorporation and oxygen metabolism between $t_{72\text{h}}$ and $t_{96\text{h}}$, again an average rate between
376 rates measured from samples taken at $t_{48\text{h}}$ and $t_{96\text{h}}$ was used for this time interval. Since
377 bacterial respiration rates were not measured, bacterial growth efficiency (BGE, expressed as a
378 percentage) was estimated based on BP (carbon units) and community respiration (CR, oxygen
379 units). As BP was determined more often than CR during the first 48 h, hourly BP rates were
380 integrated using trapezoidal integrations during the time period when CR was measured. We
381 assumed that heterotrophic prokaryotes were responsible for 70% of CR (BR/CR ratio; Lemée et
382 al., 2002) and used a respiratory quotient (RQ) of 0.8 (del Giorgio and Williams, 2005),
383 following the equation:

$$384 \quad \text{BGE} = \left(\frac{\text{BP}}{\text{CR} \times \frac{\text{BR}}{\text{CR}} \text{ratio} \times \text{RQ} + \text{BP}} \right) \times 100 \quad (8)$$

385 When BP varied following an exponential growth, we calculated growth rates (μ_{BP}) from linear
386 least square regression of \ln BP rates versus time.



387 **3. Results**

388 **3.1. Initial conditions**

389 Initial conditions in terms of the chemical and biological standing stocks measured while
390 filling the tanks at the three stations are fully described in Gazeau et al. (2020). Briefly, the three
391 experiments were conducted with surface seawater collected during stratified oligotrophic
392 conditions typical of the open Mediterranean Sea at this period of the year (Table 1). Nitrate +
393 nitrite (NO_x) concentrations were maximal at station FAST with a NO_x to dissolved inorganic
394 phosphate (DIP) molar ratio of ~ 4.6 . Very low NO_x concentrations were observed at stations
395 TYR and ION (14 and 18 nmol L^{-1} , respectively). DIP concentrations were the highest at station
396 TYR (17 nmol L^{-1}) and the lowest at the most eastern station (ION, 7 nmol L^{-1}). Consequently,
397 the lowest NO_x :DIP ratio was measured at TYR (0.8), compared to ION and FAST (2.8 and 4.6 ,
398 respectively). Silicate ($\text{Si}(\text{OH})_4$) concentrations were similar at TYR and ION ($\sim 1 \mu\text{mol L}^{-1}$) and
399 the lowest at FAST ($\sim 0.6 \mu\text{mol L}^{-1}$). Both POC and DOC concentrations were the highest at
400 station TYR (12.9 and $72.2 \mu\text{mol L}^{-1}$, respectively) and the lowest at FAST (6.0 and $69.6 \mu\text{mol}$
401 L^{-1} , respectively). Very low and similar concentrations of chlorophyll *a* were measured at the
402 three stations (0.063 - $0.072 \mu\text{g L}^{-1}$). Phytoplankton communities at stations TYR and ION were
403 dominated by Prymnesiophytes followed by Cyanobacteria, while, at station FAST, the
404 phytoplanktonic community was clearly dominated by photosynthetic prokaryotes. At all three
405 stations, the proportion of pigments representative of larger species was very small ($< 5\%$;
406 Gazeau et al., 2020). Heterotrophic prokaryotes were the most abundant at station FAST ($6.15 \times$
407 $10^5 \text{ cells mL}^{-1}$) and the least abundant at station ION ($2.14 \times 10^5 \text{ cells mL}^{-1}$).



408 Relatively similar ^{14}C -based particulate production rates were measured at the start of the
409 experiments (t_0) in the control tanks (C1 and C2) at station ION and FAST (ca. $0.014 - 0.015 \mu\text{g}$
410 $\text{C L}^{-1} \text{h}^{-1}$). At both stations, ca. 80% of the production was attributed to larger ($> 2 \mu\text{m}$) cells and
411 the percentage of extracellular release (%PER) did not exceed 45%. Lower rates were estimated
412 at station TYR (total particulate production of $0.08 \mu\text{g C L}^{-1} \text{h}^{-1}$) from which 87.5% was due to
413 large cells $> 2 \mu\text{m}$. A larger amount of ^{14}C incorporation was released as dissolved organic
414 matter at station TYR compared to the two other stations (PER ca. 60%). Metabolic balance
415 derived from oxygen measurements showed that, at all three stations, the community was net
416 heterotrophic with a higher degree of heterotrophy at station TYR (NCP were $-1.9, -0.2, -0.8$
417 $\mu\text{mol O}_2 \text{L}^{-1} \text{d}^{-1}$ at TYR, ION and FAST, respectively, as measured in the controls from seawater
418 sampled at t_0). CR and GPP rates were respectively the highest and the lowest at station TYR
419 compared to the other two stations. Finally, BP rates were the highest at station FAST (35.8 ng C
420 $\text{L}^{-1} \text{h}^{-1}$), intermediate at ION ($26.1 \text{ ng C L}^{-1} \text{h}^{-1}$) and the lowest at TYR ($21.3 \text{ ng C L}^{-1} \text{h}^{-1}$).

421 **3.2. Changes in biological stocks**

422 DOC concentrations showed a general increasing trend during the three experiments and
423 a large variability between duplicates (Fig. 2). This variability appeared as soon as 1 h after dust
424 seeding (t_{1h}) while the range of variation at t_0 (before dust seeding) was rather moderate
425 (difference between minimal and maximal values in all tanks of $1.3, 6.2$ and $4.3 \mu\text{mol C L}^{-1}$ at
426 station TYR, ION and FAST, respectively). As a consequence of this variability, no clear impact
427 of dust seeding (D) could be highlighted at station TYR and FAST. Indeed, DOC concentrations
428 in the two duplicates (D1 and D2) were higher than values in the controls (C1 and C2) in only
429 33% of the samples along the experiments (after dust seeding). In contrast, at station ION, DOC
430 concentrations appeared impacted by dust seeding as higher concentrations were almost



431 systematically (83% of the time after dust seeding) measured for this treatment as compared to
432 control tanks at the same time. At all stations, this impact was somewhat exacerbated under
433 conditions of temperature and pH projected for 2100 (G1 and G2) as DOC concentrations were
434 almost all the time higher in these tanks than in control tanks (83 - 100% of the samples after
435 dust seeding, depending on the station).

436 Total hydrolysable carbohydrates and amino acids concentrations along the three
437 experiments are shown in Fig. S2. TCHO concentrations were quite variable between tanks
438 before dust seeding (t_0 ; 649 - 954, 569 - 660 and 600 - 744 nmol L^{-1} at station TYR, ION and
439 FAST, respectively) and no visible impact of the treatments were visible at station TYR (TCHO
440 tended to decrease everywhere). In contrast, at station ION and FAST, values in dust amended
441 tanks increased and appeared higher than in control tanks towards the end of the experiments
442 although the large variability between duplicates tended to mask this potential effect. An impact
443 of dust seeding was much clearer for TAA concentrations that showed larger increases
444 throughout the three experiments in tanks D1 and D2 as compared to control tanks, this effect
445 being exacerbated for warmer and acidified tanks (G1 and G2). The ratio between TAA and
446 DOC concentrations (Fig. 2) showed increasing trends in tanks D and G during all three
447 experiments with a clear distinction between treatments at the end of the experiments ($G > D >$
448 C). The strongest increase was observed at station FAST in tanks G where final values were
449 above 3%.

450 Particulate organic carbon (POC) concentrations strongly decreased at all stations
451 between $t-12\text{h}$ and t_0 , this decrease being the largest at station TYR where concentrations
452 dropped from 25.7 to 9.6 - 13.2 $\mu\text{mol C L}^{-1}$ (Fig. 3). After dust seeding, POC concentrations did
453 not show clear temporal trends for the three experiments although a slight general increase could



454 be observed at station FAST. Furthermore, no impact of dust seeding and warming/acidification
455 could be observed for this parameter. While concentrations of transparent exopolymer particles
456 (TEP-C) were rather constant through time in control tanks at the three stations, a large increase
457 was observed in dust-amended tanks (D and G) with TEP-C reaching values up to $\sim 2 \mu\text{mol C L}^{-1}$
458 in tank G1 at station TYR after 24 h (i.e. $\sim 17\%$ of POC concentration, Fig. 3). In all cases except
459 for tank G2 at station ION, TEP-C further decreased towards the end of the experiments although
460 concentrations remained well above those observed in the controls. As the variability between
461 duplicated tanks G was rather high, no impact of warming/acidification on TEP dynamics could
462 be highlighted at the three stations.

463 **3.3. Changes in metabolic rates**

464 ^{14}C -based particulate production rates as measured during the different time intervals at
465 the three stations were low in control tanks (maximal total particulate production of $0.34 \mu\text{g L}^{-1}$
466 h^{-1} at station FAST) and did not show any particular temporal dynamics (Fig. 4). In these tanks,
467 the vast majority of particulate production was attributed to cells above $2 \mu\text{m}$ (65 - 89%). The
468 percentage of extracellular release (%PER) was overall maximal at station TYR and minimal at
469 station FAST with a tendency to decrease with time at the three stations although large variations
470 were observed between duplicates.

471 Dust addition alone did not have any clear positive impact on all ^{14}C -based rates at
472 station TYR, with even an observable decrease in production rates from larger cells ($> 2 \mu\text{m}$)
473 compared to the controls. In contrast, at this station, dust seeding under warmer and acidified
474 conditions (tanks G) had a positive effect on particulate production rates, this effect being
475 particularly visible for cells $< 2 \mu\text{m}$ and to a lesser extent on dissolved production with a general



476 decrease of %PER. An important discrepancy between the duplicates of treatment G was
477 observable at the end of the experiment with much larger rates measured in tank G2.

478 In contrast to station TYR, an enhancement effect of dust addition was clearly visible at
479 station ION where all rates increased towards the end of this experiment reaching a maximal
480 total particulate production of $0.6 - 0.7 \mu\text{g L}^{-1} \text{h}^{-1}$ in tanks D1 and D2. Since this positive effect
481 was similar between small and larger cells, dust addition alone had no effect on the partitioning
482 of production at this station, with cells $> 2 \mu\text{m}$ representing $\sim 80\%$ of total production. Although
483 being also positively impacted and increasing with time, dissolved production appeared less
484 sensitive than particulate production leading to an overall decrease of %PER at this station
485 following dust addition. These positive impacts of dust seeding on ^{14}C -based particulate
486 production rates were even more visible at this station under warmer and acidified conditions
487 (tanks G) with maximal rates more than doubled compared to those measured under present
488 conditions of temperature and pH ($1.5 - 1.6 \mu\text{g L}^{-1} \text{h}^{-1}$). Dust seeding under warmer and acidified
489 conditions had a slight impact on the partitioning of particulate production at this station with
490 smaller cells benefiting the most from these conditions. %PER remained between 20 and 30%.

491 At station FAST, similarly to station ION, total particulate production rates were clearly
492 enhanced by dust addition (tanks D) reaching maximal values during the incubation time interval
493 t48 - 56h. No clear increase was observed for total particulate production on the next incubation
494 (t96 - 120h) while production rates of cells larger than $2 \mu\text{m}$ increased and rates of smaller cells
495 decreased. However at FAST, in contrast to station ION, there was much less impact of
496 warming/acidification on all measured rates although rates measured on smaller cells ($< 2 \mu\text{m}$)
497 did not decrease at the end of the experiment as observed under present environmental



498 conditions. %PER under both present conditions of temperature and pH (tanks D) decreased
499 during this experiment reaching values lower than in the controls and in tanks G.

500 The initial enrichment of the tanks in ^{13}C -bicarbonate led to an increase in the ^{13}C
501 signature of dissolved inorganic carbon ($\delta^{13}\text{C-C}_T$) of above 300‰, with generally lower values
502 measured in warmer and acidified tanks (G; Fig. S3). After this initial enrichment, $\delta^{13}\text{C-C}_T$ levels
503 decreased linearly in all tanks. At stations TYR and ION, the isotopic signature of dissolved
504 organic carbon ($\delta^{13}\text{C-DOC}$; Fig. S3) increased with time, although these increases were rather
505 low and limited to $\sim 4\%$ over the course of the experiments. In contrast to station TYR, at ION,
506 an enhanced incorporation of ^{13}C into DOC was visible after 24 h in tanks D and G in
507 comparison to control tanks. A similar observation was done at station FAST, especially at the
508 end of the experiment, although much more variability was observed at this station.

509 The incorporation of ^{13}C onto particulate organic carbon ($\delta^{13}\text{C-POC}$) is shown in Fig. 5.
510 At all stations, $\delta^{13}\text{C-POC}$ increased with time but reached lower enrichment levels at station
511 TYR as compared to ION and FAST. At this station, incorporation rates appeared smaller in
512 dust-amended tanks under present environmental conditions (tanks D). As for ^{14}C -based
513 production rates, an important discrepancy was observed between duplicates under future
514 conditions of temperature and pH (tanks G) with much higher final $\delta^{13}\text{C-POC}$ at the end of the
515 experiment in tank G2. At station ION, enrichment levels obtained at the end of the experiment
516 were more important in dust-amended tanks reaching maximal levels of 73‰ in tank G2 at t72h.
517 This enhancement effect was even more visible at station FAST with maximal enrichment levels
518 of 146‰ (tank D2 at t96h). Since no sampling occurred at t72h, these enrichment levels cannot
519 be directly compared to what was measured at station TYR and ION. However, by interpolating



520 values at t72h assuming a linear increase between these time intervals, enrichment levels
521 appeared similar although slightly higher for tanks D between station ION and FAST.
522 NCP rates as measured using the O₂ light-dark method showed that, under control
523 conditions, the communities remained the vast majority of the time throughout the three
524 experiments in a net heterotrophic state (NCP < 0; Fig. 6). This was especially true at station
525 TYR where the lowest NCP rates were measured. At this station, dust addition whether under
526 present or future conditions of temperature and pH did not switch the community towards net
527 autotrophy but even drove the community towards a stronger heterotrophy. This was related to
528 the fact that while gross primary production rates were not positively impacted, community
529 respiration increased in tanks D and G. At station ION, dust addition alone (tanks D) led to a
530 switch from net heterotrophy to net autotrophy after two days of incubation due to a stronger
531 positive effect of dust on GPP than on CR. Under future environmental conditions (tanks G), the
532 same observation was made with higher NCP and GPP rates than in tanks D. CR rates reacted
533 quickly to these forcing factors in tanks G and initially (first incubation) drove the community
534 towards a much stronger heterotrophy as compared to the other tanks. Finally, at station FAST,
535 similarly to what was observed at ION, the community became autotrophic after two days of
536 incubation in dust amended tanks as, although both GPP and CR were positively impacted by
537 dust addition, this impact was less important for CR. Warming and acidification had a limiting
538 impact on this enhancement, with a lower final NCP in tanks G compared to tanks D, a
539 difference that can be related to an absence of effects of these environmental stressors on GPP
540 while CR clearly increased at higher temperature and lower pH.

541 While BP remained constant or gradually increased in control tanks depending on the
542 station, a clear and quick fertilization effect was observable following dust addition (treatment D



543 and G) at all stations (Fig. 7). At station TYR, BP rates sharply increased to reach maximal
544 values at t24h, with an even stronger increase observed under warmer and acidified conditions
545 (tanks G). After this initial increase, rates slightly decreased towards the end of the experiment.
546 This fertilization effect appeared less important at station ION where lower maximal rates were
547 obtained after 24 h as compared to station TYR. Nevertheless, the same observations can be
548 made, namely, 1) higher rates were measured under future temperature and pH levels and 2) after
549 this initial sharp increase, rates gradually decreased towards the end of the experiment especially
550 in tanks G. At station FAST, a much stronger effect of warming/acidification was observed with
551 an important increase of BP in tanks G until 24 or 48 h post-seeding, depending on the duplicate.
552 A sharp decline was observed for this treatment until the end of the experiment although rates
553 remained higher than those measured in tanks C and D. The impact of dust addition under
554 present environmental conditions (tanks D) was somehow more limited than at the other stations
555 with a gradual increase until t72h with maximal rates ~ 40 - 100% higher than rates measured in
556 the controls. However, BP increased exponentially between t0 and t12h in all tanks including
557 controls, and in all experiments (Table 2). The growth rate of BP (μ_{BP}) in control tanks was the
558 highest at TYR, intermediate at ION and the lowest at FAST. μ_{BP} increased significantly in all
559 dust amended tanks compared to controls. Under future environmental scenarios, μ_{BP} tended to
560 increase compared to treatment D but with a variable relative change.

561 BGE increased in dust amended tanks under present environmental conditions (treatment
562 D) at TYR and ION, while no changes were detectable at station FAST due to a strong
563 discrepancy between control duplicates and overall higher BGE at this station in the controls
564 (Table 3). In contrast, warming and acidification exerted the strongest effect at station FAST
565 with a doubling of BGE between treatment G and D. Although an increase in BGE was also



566 observed at the two other stations in treatment G as compared to present environmental
567 conditions (treatment D), this increase was more limited (ca. 1 to 1.4-fold increase).

568 The alkaline phosphatase Vm (AP Vm) increased in all experiments after dust seeding,
569 with amplified effects in G treatments (Fig. S4). Note that AP Vm increased also in the controls
570 at TYR and FAST. In contrast, leucine aminopeptidase Vm (LAP vm) showed succession of
571 peaks instead of continuously increasing (Fig. S4). It was higher in dust alone treatment (D) as
572 compared to the controls at TYR and FAST. A larger variability between duplicates at ION
573 prevents such an observation. At all stations, maximum velocities were measured under future
574 environmental conditions (G). Vm being possibly influenced by enzyme synthesis but also by the
575 number of cells inducing such enzymes, we computed also specific AP Vm per heterotrophic
576 bacterial cell (Fig. 7). Specific AP Vm slightly increased during all experiments in controls and
577 dust-amended tanks (D) with no visible differences between these treatments, a clear over-
578 expression of this enzyme was observed under warmer and more acidified conditions (treatment
579 G) especially at station FAST where velocities were enhanced by a ~8-fold at t96h.

580 **3.4. Inorganic and organic material export**

581 Both total mass and organic matter fluxes, as measured from analyses of the sediment
582 traps at the end of each experiment, were extremely low under control conditions (Fig. 8).
583 Additions of dust in tanks D and G led to a strong increase in both fluxes with a large variability
584 between the duplicates of treatment D at ION. No clear changes between tanks maintained under
585 present and future conditions of temperature and pH could be highlighted.



586 4. Discussion

587 4.1. Initial conditions of the tested waters and evolution in 588 controls

589 As discussed in the companion paper from Gazeau et al. (2020), the three sampling
590 stations were typical of stratified oligotrophic conditions encountered in the open Mediterranean
591 Sea in late spring / early summer. DOC concentrations at the start of the experiments were in the
592 same range ($60 - 75 \mu\text{mol C L}^{-1}$) as those measured from samples collected in surface waters
593 using clean sampling procedures (Van Wambeke et al., 2020b), revealing no contamination
594 issues from our sampling device. TAA concentrations as measured in the tanks at t_0 were also
595 consistent with measurements from surface water samples (Van Wambeke et al., 2020b) with an
596 average across stations and treatments of $254 \pm 36 \text{ nmol L}^{-1}$ (Fig. S2). In contrast, TCHO
597 appeared higher at t_0 (average across stations and treatments of $681 \pm 98 \text{ nmol L}^{-1}$) than
598 concentrations based on clean *in situ* sampling (average of $595 \pm 43 \text{ nmol L}^{-1}$; Van Wambeke et
599 al., 2020b). The decrease in POC concentrations between pumping ($t-12\text{h}$) and t_0 for the three
600 experiments, especially at station TYR (likely linked to higher initial concentrations), was likely
601 a consequence of sedimentation of senescent cells and/or fecal pellets in our experimental
602 systems, which are designed to evaluate the export of matter thanks to their conical shape. TEP
603 concentrations were not quantified at $t-12\text{h}$ and therefore there is no possibility to evaluate if
604 sedimentation of these particles occurred before t_0 in our tanks. At t_0 , larger and more abundant
605 TEP were measured at station TYR compared to the two other stations (data not shown) leading
606 to a larger contribution of TEP carbon content (TEP-C) to POC concentrations (Fig. 3).



607 As a consequence of a very low availability in inorganic nutrients, TChl a and ^{14}C -based
608 production rates were very low, all typical of oligotrophic conditions. Nano- and micro-
609 phytoplanktonic cells ($> 2 \mu\text{m}$) contributed most of the ^{14}C -based particulate production ($\sim 80\%$),
610 as found also on several on-deck incubations at the three stations (on average $73 \pm 6\%$; Marañón
611 et al., 2020). %PER values were also very similar to those measured during these on-deck
612 incubations ($\sim 40\text{-}45\%$; see Marañón et al., 2020). This suggests no significant impact of our
613 experimental protocol on rates and partitioning of ^{14}C -based production rates (i.e. sampling from
614 the continuous seawater supply, delay of 12 h before initial measurements, artificial light etc.).
615 The low values of chlorophyll stocks as well as of ^{14}C -based production rates are consistent with
616 previous estimates based on direct measurements, satellite observations and modelling
617 approaches in the same areas in late spring / early summer (e.g. Bosc et al., 2004; Lazzari et al.,
618 2016; Moutin and Raimbault, 2002).

619 The metabolic balance was in favor of net heterotrophy at all stations at the start of the
620 experiments (NCP < 0). Net heterotrophy in the open Mediterranean sea at this period of the year
621 has been reported by Regaudie-de-Gioux et al. (2009) and Christaki et al. (2011) in agreement
622 with our measurements at t_0 in control tanks (Table 1). The lowest NCP and the highest CR rates
623 were measured at station TYR, suggesting that the autotrophic plankton community was not very
624 active at this station. This was confirmed by the ^{14}C -based particulate production rates, which
625 were about half the ones measured at the other two stations. The community at TYR was most
626 likely relying on regenerated nutrients, as shown by the highest levels of ammonium (NH_4^+)
627 measured at the start of this experiment (Gazeau et al., 2020). As discussed in Guieu et al.
628 (2020), a dust deposition event took place several days before the arrival of the vessel in this
629 area, likely on May 10-12. This dust event was confirmed by inventory of particulate aluminium



630 in the water column at several stations of the Tyrrhenian Sea including TYR, 6 to 9 d after the
631 event (Matthieu Bressac, pers. comm.). This dust deposition likely stimulated phytoplankton
632 growth and POC accumulation shortly after the deposition and consequently increased the
633 abundance of herbivorous grazers (copepods) and attracted carnivorous species (Feliú et al.,
634 2020), subsequently driving the community towards a net heterotrophic state that characterized
635 the initial condition of the experiment at this station. The optimal conditions for BP growth at
636 this station were also confirmed by the highest μ_{BP} growth rates obtained among the three
637 experiments (Table 2; 0.06 - 0.07 h⁻¹) in controls tanks.

638 The two other stations, although both also showing a slight net heterotrophic state, were
639 clearly different from each other in terms of initial biological stocks and metabolic rates. Indeed,
640 whereas TChla and abundances of pico- and nano-autotrophic cells (flow cytometry counts;
641 Gazeau et al., 2020) were higher at FAST compared to ION, the autotrophic community was not
642 more efficient at fixing carbon at this station, as shown by similar initial ¹⁴C-based production
643 rates. In contrast, both heterotrophic prokaryotic abundances and BP were much higher at station
644 FAST as compared to ION, leading to initial higher CR and lower NCP. At ION, the initial NCP
645 closer to metabolic balance further suggests a tight coupling between heterotrophic prokaryotes
646 and phytoplankton at this station, as discussed by Dinasquet et al. (2021).

647 For most of the chemical and biological stocks (e.g. nutrients, pigments etc.) presented in
648 Gazeau et al. (2020), no major changes took place during the three experiments under control
649 conditions. Here, we further show that DOC, POC as well as TEP concentrations did not exhibit
650 strong changes during the experiments. For DOC, large variability between the duplicates (C1
651 and C2) potentially masked an increase towards the end of the experiments. The same holds true
652 for autotrophic metabolic rates, as ¹⁴C-based particulate production rates showed no marked



653 variations during the three experiments, although a slight increase was visible at FAST until
654 t48h. The communities at the three stations remained heterotrophic under the nutrient-limited
655 conditions in the controls. However, heterotrophic prokaryotes probably benefited from initial
656 inputs of available organic matter issued from other stressed eukaryotic organisms and/or POC
657 decay between t-12h and t0, which could be due to both sedimentation and degradation. This was
658 reflected in the progressive increase of BP, their variable initial growth rates (μ_{BP} ranged from
659 0.02 to 0.06 h⁻¹ in control tanks according to the experiment) as well as increasing TAA/DOC
660 ratios at the three stations. Finally, an initial increase of BP during incubations is generally
661 described and classically attributed to a bottle effect, which favours large, fast-growing bacteria
662 and often induces mortality of some phytoplankton cells (Calvo-Díaz et al., 2011; Ferguson et
663 al., 1984; Zobell and Anderson, 1936)

664 **4.2. Impact of dust addition under present environmental** 665 **conditions**

666 The addition of nitrogen and phosphorus in the experimental tanks through dust seeding
667 (+ 11 to + 11.6 $\mu\text{mol L}^{-1}$ and + 22 to + 30.8 nmol L^{-1} for NO_x and DIP, respectively, in dust
668 enriched, i.e. D1 and D2, versus controls; Gazeau et al., 2020) had very contrasting impacts on
669 the metabolism of the communities, depending on the station. At TYR, surprisingly, the relieving
670 of nutrient limitation had a negative impact on ¹³C incorporation as well as on both particulate
671 and dissolved ¹⁴C-based production rates (as seen by the relative changes compared to the
672 control presented in Fig. 9). These observations are fully corroborated by the observed relative
673 decrease in GPP in these tanks (D1 and D2) relative to controls and by the negative impact of
674 dust-addition on TChla concentrations as discussed by Gazeau et al. (2020). Integrated ¹⁴C-



675 incorporation rates converted to P (using a C:P molar ratio of 245:1 determined in the particulate
676 organic matter in surface waters of the Northwestern Mediterranean Sea during stratification;
677 Tanaka et al., 2011) showed that phytoplankton P requirements in treatment D ($\sim 2 \text{ nmol P L}^{-1}$)
678 were much lower than the release of DIP through dust addition at this station (+ 20.4 to + 24.6
679 nmol P L^{-1} ; Gazeau et al., 2020). This suggests that the observed strong decrease of DIP at this
680 station following dust addition was due to an utilization by the heterotrophic compartment.
681 Indeed, in contrast to the autotrophic compartment, both heterotrophic prokaryotic abundances
682 (Gazeau et al., 2020) and BP (this study, Fig. 9) showed that heterotrophic prokaryotes reacted
683 quickly and strongly to the increase in DIP availability. Integrated BP increased by almost 400%
684 in tanks D1 and D2 as compared to controls (Fig. 9). Such relative increases of BP surpassing by
685 far the observed relative increases of CR suggest a much more efficient utilization of resources
686 by heterotrophic prokaryotes in this treatment (i.e. BGE increased by 200% as compared to the
687 controls; Fig. 9). As such, at this station, the addition of dust drove the community to an even
688 more heterotrophic state. Such absence of response of the autotrophic community despite the
689 input of new N and P from simulated wet deposition was never observed in dust enrichment
690 experiments performed in the Mediterranean Sea (Guieu and Ridame, 2020). To the best of our
691 knowledge, it is the first time that a negative effect of dust addition is experimentally
692 demonstrated on the metabolic balance. The apparent utilization of nutrients, especially DIP
693 (Gazeau et al., 2020), by heterotrophic prokaryotes was extremely fast, starting right after dust
694 addition and driving DIP concentrations back to control levels at the end of the experiment
695 (t72h). While heterotrophic prokaryotic abundances increased until the end of the experiment,
696 BP rates increased exponentially during the first 24h, and then BP reached a plateau.
697 Heterotrophic prokaryotes appeared limited by nutritive resources although DIP concentrations



698 were not yet back to their initial level and no relative increase of the AP Vm per cell compared to
699 the control was observed in these tanks. Independent nutrient experiments showed a direct
700 stimulation of BP in the dark after addition of DIP (Van Wambeke et al., 2020b), suggesting a
701 great competition with phytoplankton for DIP utilization at TYR. After 24 h, abundances of
702 heterotrophic prokaryotes continued to increase while BP stabilized, suggesting a less extent of
703 lysis and viral control than in the other experiments (abundances of heterotrophic nanoflagellates
704 decreased; Dinasquet et al., 2021). This limitation of BP was potentially a consequence of
705 relatively less available access to labile DOC sources, as ^{14}C -based production rates decreased
706 relative to the controls at t24h and t48h although BP increased by 200 - 800%. The very tight
707 coupling between phytoplankton and bacteria at all stations investigated was further confirmed
708 by the absence of an important ^{13}C incorporation into DOC (Fig. S3).

709 At stations ION and FAST, in contrast to TYR, both the autotrophic and heterotrophic
710 community benefited from dust addition relative to the controls (Fig. 9). Interestingly, while the
711 relative increase in integrated autotrophic processes (GPP and all ^{14}C -based production rates)
712 was more important at FAST than at ION, the opposite was observed for BP. Estimated BGE
713 values even suggest an absence of response to dust addition at station FAST compared to the
714 controls. The different (relative) responses of BP at the two stations could be partly explained by
715 the dynamics of BP in the control tanks as no clear pattern could be observed at ION while a
716 continuous increase was observed at FAST. As shown by Gazeau et al. (2020), at FAST,
717 abundances of heterotrophic prokaryotes were much higher at the start of the experiment, further
718 increased until t48h and then declined until the end of the experiment.

719 We can rule out a potential limitation of BP from DIP availability at station FAST as DIP
720 levels remained much higher in tanks D than in the controls (Gazeau et al., 2020). Furthermore,



721 the amount of maximum DIP reached before its decline compared to TYR and ION showed a
722 less important direct DIP uptake, suggesting that communities were not as much P limited at
723 FAST compared to the other stations at the start of the experiment. Finally, no increase of
724 specific AP Vm was observed in these tanks as compared to the controls (Fig. 7), suggesting no
725 particular additional needs for AP synthesis per unit cell following dust addition. A potential
726 explanation resides in the competition between heterotrophic bacteria and phytoplankton for DIP
727 utilization. At station ION, P requirements of the autotrophic community were low compared to
728 the initial input of DIP following dust seeding ($\sim 9 \text{ nmol P L}^{-1}$ as compared to an input of + 22 to
729 + 23.3 nmol P L^{-1} ; Gazeau et al., 2020). In contrast, at FAST, the autotrophic community
730 consumed a much larger proportion of the initial DIP input ($\sim 25 \text{ nmol P L}^{-1}$ as compared to an
731 input of 30.8 - 31.3 nmol P L^{-1}) and phytoplankton appeared as a winner for the utilization of
732 DIP towards the end of the experiment at this station. It seems that heterotrophic bacteria and
733 phytoplankton were more in a steady state of equilibrium and less stressed at the start of the
734 experiment at FAST, i.e. phytoplankton abundances showed no decrease between t-12h and t0
735 and BP did not increase as much as during the other two experiments, suggesting a strong
736 predation pressure (μ_{BP} was the lowest of the three experiments: ca. 0.02 h^{-1} in the controls).

737 The explanation for the observed differential responses of the autotrophic community at
738 the two stations (FAST > ION) is not evident and further complicated by the fact that the
739 sampling strategy differed between the two stations (i.e. no sampling at t72h, replaced by a
740 sampling at t96h). It is however unlikely that this different sampling strategy was responsible for
741 the different changes in computed integrated autotrophic rates at the two stations. As a maximal
742 increase in nano-eukaryote abundance was observed at t72h at FAST (followed by a drastic
743 reduction at t96h; Gazeau et al., 2020), excluding this sampling point in the calculation of



744 autotrophic metabolic rates would most likely have led to an underestimation of these rates rather
745 than an overestimation. Furthermore, a similar partitioning of ^{14}C -based production rates
746 throughout the two experiments did not provide clear insights on which size-group benefited the
747 most at station FAST compared to ION. Two non-exclusive explanations could be proposed: (1)
748 as mentioned above, a less important immediate consumption of DIP by heterotrophic bacteria
749 leading to a higher availability of new DIP for phytoplankton growth at FAST (+ 31 vs + 22 to +
750 23 nmol L^{-1} at FAST and ION, respectively; Gazeau et al., 2020) along with (2) the presence of a
751 potentially more active community at the start of the experiment at FAST with a much higher
752 contribution from smaller cells (i.e. pico-eukaryotes, *Synechococcus*; Gazeau et al., 2020) that
753 are well known to be better competitors for new nutrients and that were less stressed at the start
754 of the experiments (e.g. Moutin et al., 2002).

755 During both experiments at ION and FAST, communities switched from net heterotrophy
756 to net autotrophy between 48 and 72 h following dust addition (Fig. 6), leading to a positive
757 integrated NCP at both stations (Fig. 9). This is an important observation since, to the best of our
758 knowledge, the present study constitutes the first investigation of the community metabolism
759 response to dust addition. However, it is important to discuss the timing of such a switch in
760 community metabolism. Since heterotrophic prokaryotes reacted faster than autotrophs to the
761 relief of nutrient limitation (i.e. BP already increased by 150-500% at t24 h, while ^{14}C -based
762 production rates increased only after 48-72 h), NCP was first lower (and negative) in the dust-
763 amended tanks as compared to the controls. Marañón et al. (2010) and Pulido-Villena (2008,
764 2014) have already reported on a much faster response of the heterotrophic prokaryote
765 community to dust enrichment in the central Atlantic Ocean and Mediterranean Sea,
766 respectively. As DIP concentrations at the completion of their 48 h incubations did not differ



767 from that in the controls, it is unlikely that primary production rates and consequently NCP
768 would have further increased. In contrast, during our experiments, DIP concentrations in dust-
769 amended tanks (D) reached initial levels only after 72 h at TYR and ION and remained far above
770 ambient levels at FAST until the end of the experiment (t96h). During the PEACETIME cruise,
771 high frequency sampling of CTD casts allowed following the evolution of biogeochemical
772 properties and fluxes before and after wet dust deposition that took place in the area around
773 FAST on June 3-5 (Van Wambeke et al., 2020a). As in our experiment, a rapid increase in BP
774 was responsible for the observed *in situ* decline in DIP concentrations in the mixed layer
775 following the rain with no detectable changes in primary production (Van Wambeke et al.,
776 2020a). The intensity of the wet deposition event that was simulated during our experiments was,
777 by far, more important, but still representative of a realistic scenario (Bonnet and Guieu, 2006;
778 Loÿe-Pilot and Martin, 1996; Ternon et al., 2010).

779 The most intriguing result concerning the export of inorganic and organic matter is that
780 these fluxes were maximal at the end of the experiment at TYR in the dust-amended tanks
781 despite the fact that ¹⁴C-based production was relatively low and not enhanced by dust addition.
782 Based on previous studies (Bressac et al., 2014; Louis et al., 2017; Ternon et al., 2010), organic
783 matter export was most likely mainly due to the formation of organic-mineral aggregates
784 triggered by the introduced lithogenic particles (referred thereafter to as POC_{litho}). Indeed, Louis
785 et al. (2017) showed that such an aggregation process occurs within 1 h after dust deposition.
786 These authors further demonstrated the key role of TEP as the conversion of dissolved organic
787 matter (DOM) to POC was mediated by TEP formation/aggregation activated by the introduction
788 of dust. As TEP concentrations were only measured on two occasions after seeding with the first
789 measurement occurring at t24h,), it prevents studying in detail the dynamics of these particles.



790 Nevertheless, it is very likely that the sharp decrease of TEP abundances (data not shown)
791 between t_{24h} and t_{72h} was related to POC_{litho} export. The coefficient linking POC_{litho} to $Litho_{flux}$
792 (i.e. the mass of sedimented particles) measured here (0.02) is consistent with values reported for
793 other experiments conducted in the Mediterranean Sea (Louis et al., 2017).

794 Even though ^{14}C -based production rates were enhanced in the dust-amended tanks at
795 stations ION and FAST, the amount of POC exported at the end of these experiments remained
796 lower than at TYR, with fluxes ~ 10 - $20 \text{ mg C m}^{-2} \text{ d}^{-1}$. It must be stressed that not all the
797 lithogenic material introduced in the tanks was recovered after 4 (and 5) days, with the highest
798 percentage ($\sim 30\%$) being found at TYR, indicating that the tested waters at this station had a
799 better capacity to aggregate dust. This efficiency to export POC_{litho} more rapidly at TYR
800 compared to ION and FAST was likely due to the age and quantity of dissolved organic matter
801 present at the time of the seeding (Bressac and Guieu, 2013). At TYR, impacted by a strong dust
802 event several days before the experiment started (see above), the likely stimulation of the
803 autotrophs after this *in situ* event should have been followed by the production of a fresh and
804 abundant DOM, comparable to the “post-bloom situation” in Bressac and Guieu (2013).

805 **4.3. Impact of dust addition under future environmental** 806 **conditions**

807 Warming and/or acidification had a clear impact on most evaluated stocks and metabolic
808 rates. Gazeau et al. (2020) have already discussed temperature/pH mediated changes in nutrient
809 uptake rates and autotrophic community composition in these experiments. The difference in the
810 relative response of plankton communities to dust addition under present and future conditions of
811 temperature and pH was highly dependent on the sampling station (Fig. 9). At all stations, ^{14}C -



812 based particulate production rates were enhanced under future conditions as compared to those
813 measured under present environmental conditions (treatment D) although this pattern was not
814 observed for ^{13}C incorporation into POC at stations ION and FAST. At ION, no differences
815 could be detected and at FAST an even lower ^{13}C -enrichment was measured at the end of the
816 experiment. These contrasting patterns between ^{14}C -uptake rates and ^{13}C -enrichment of POC are
817 likely explained by the fact that the latter covered the whole experimental period (including dark
818 periods) and represents net community carbon production while ^{14}C -based rates were measured
819 over 8 h incubations in the light, providing an estimate in between gross and net carbon
820 production.

821 Similarly, the heterotrophic compartment was more stimulated, as BP rates increased
822 strongly at all stations under this treatment compared to treatment D. The relatively smaller
823 increase in CR rates, compared to BP, leading to higher BGE suggests a better utilization of
824 resources by heterotrophic prokaryotes under future environmental conditions. Overall, CR was
825 more impacted than GPP, with the consequence that all integrated NCP rates decreased under
826 future environmental conditions compared to present conditions (treatment D). At station TYR,
827 as discussed previously, dust addition under present conditions did not lead to a switch from net
828 heterotrophy to net autotrophy. This pattern was even more obvious under warmer/acidified
829 conditions, with a larger decrease in integrated NCP at this station. The decrease of integrated
830 NCP at station FAST relative to controls, as well as the smaller increase of all ^{14}C -based
831 production rates relative to those observed at station ION must be taken with caution. As already
832 discussed, the fact that for these processes (O_2 metabolism and ^{14}C -incorporation), no samples
833 were taken at FAST at $t_{72\text{h}}$ when maximal cell abundances were recorded for all autotrophic
834 groups (pico- and nano-eukaryotes, autotrophic bacteria) must have artificially led to an



835 underestimation of these integrated metabolic rates. The question of the timing appeared even
836 more preponderant under warmer/acidified conditions, especially at station FAST, where the
837 very important increase in BP led to a full consumption of DIP before t48h (Gazeau et al., 2020)
838 and drove the community towards a strong heterotrophy. The metabolic balance further switched
839 to a slight autotrophy at t72h when heterotrophic bacterial activity appeared limited by nutrient
840 availability.

841 Both elevated partial pressure of CO₂ ($p\text{CO}_2$) and warming are major global change
842 stressors impacting marine communities. Elevated $p\text{CO}_2$ may directly facilitate oceanic primary
843 production through enhanced photosynthesis (Hein and Sand-Jensen, 1997; Riebesell et al.,
844 2007) although the effects appear to be species- and even strain-specific (e.g. Langer et al.,
845 2009). Warming affects organisms by enhancing their metabolic rates (Brown et al., 2004;
846 Gillooly et al., 2001). Although recent studies suggest large differences in temperature sensitivity
847 between phytoplankton taxa (Chen and Laws, 2017) and no significant overall difference
848 between algae and protozoa (Wang et al., 2019), mineralization rates are usually believed to be
849 more impacted by warming than primary production rates, potentially leading to a decline in net
850 oceanic carbon fixation (Boscolo-Galazzo et al., 2018; Garcia-Corral et al., 2017; Lopez-Urrutia
851 and Moran, 2007; Regaudie-de-Gioux and Duarte, 2012) and carbon export efficiency (Cael et
852 al., 2017; Cael and Follows, 2016). Overall, our experimental set-up did not allow discriminating
853 warming from acidification effects, precluding an evaluation of their potential individual
854 impacts. Nevertheless, we could speculate to which extent a 3 °C warming and a doubling of
855 CO₂ can explain some of the observed differences between D and G (for instance, a 2-fold
856 increase in ¹⁴C-based production rates at ION). For photosynthesis, meta-analysis studies
857 indicate minor effects of $p\text{CO}_2$ on most investigated species (Kroeker et al., 2013; Mackey et al.,



858 2015). Recent studies show a strong, although species-dependent, temperature sensitivity of
859 phytoplankton growth (Chen and Laws, 2017; Wang et al., 2019), suggesting that a 3 °C
860 warming could explain most of the increased carbon fixation in G compared to D. With respect
861 to NCP, our results are in line with the general view and suggest a weakening of the so-called
862 fertilization effect of atmospheric deposition in the coming decades.

863 In contrast, we did not observe an additional impact of future environmental conditions
864 on the export of organic matter after dust addition as, at each station, this export was of the same
865 order of magnitude for treatments D and G. This result is in agreement with the findings of a
866 similar experiment in coastal Mediterranean waters that considered only pH change (Louis et al.,
867 2017) but stands in contrast with the findings of Müren et al. (2005) who showed a clear
868 decrease in sedimentation following a 5 °C warming in the Baltic Sea. Only a few studies have
869 addressed the combined effect of both temperature and pH changes on aggregation processes and
870 export but none considered dust as the particulate phase. These studies, focused mainly on the
871 formation of TEP, were inconclusive on the impact of these combined factors (Passow and
872 Carlson, 2012, and references therein). As the potential effect of warming and acidification on
873 biogenic carbon export was certainly, over the rather restricted duration of the experiments,
874 insignificant as compared to the large amount of carbon exported through the lithogenic pump,
875 observations over longer temporal scales are probably required to ascertain the interactive effects
876 of these stressors in the coming decades.



877 **5. Conclusion**

878 Although the three experiments were conducted under rather similar conditions in terms
879 of nutrient availability and chlorophyll stock of the tested seawater, contrasting responses were
880 observed following the simulation of a wet dust deposition event. Under present conditions of
881 temperature and pH, at the site where the community was the most heterotrophic (TYR), no
882 positive impact of new nutrients could be observed on autotrophs, while a fast and strong
883 response of heterotrophic bacteria drove the metabolic balance towards an even more
884 heterotrophic state. The situation was different at the two other stations where a more active
885 autotrophic community responded quickly to the relief in nutrient limitation, driving the
886 community to an autotrophic state at the end of these experiments. In all tested waters, an overall
887 faster response of the heterotrophic prokaryote community, as compared to the autotrophic
888 community, was observed after new nutrients were released from dust. Phytoplankton could
889 benefit from nutrient inputs, only if the amount released from dust was enough to sustain both
890 the fast bacterial demand and the delayed one of phytoplankton. As our experimental protocol
891 consisted in simulating a strong, although realistic, wet dust deposition, further work should
892 explore at which flux a wet dust deposition triggers an enhancement of net community
893 production and therefore increases the capacity of the surface oligotrophic ocean to sequester
894 atmospheric CO₂. This question, of the utmost importance in particular for modelling purposes,
895 should be answered through future similar experiments as the ones considered in our study but
896 following a gradient approach of dust fluxes. As a consequence of a stronger sensitivity of
897 heterotrophic prokaryotes to temperature and/or pH, the ongoing warming and acidification of
898 the surface ocean will result in a decrease of the dust fertilization of phytoplankton in the coming
899 decades and a weakening the CO₂ sequestration capacity of the surface oligotrophic ocean.



900 **Data availability**

901 All data and metadata will be made available at the French INSU/CNRS LEFE CYBER database
902 (scientific coordinator: Hervé Claustre; data manager, webmaster: Catherine Schmechtig).
903 INSU/CNRS LEFE CYBER (2020)

904 **Author contributions**

905 FG and CG designed and supervised the study. All authors participated in sample analyses. FG
906 wrote the paper with contributions from all authors.

907 **Financial support**

908 This study is a contribution to the PEACETIME project (<http://peacetime-project.org>), a joint
909 initiative of the MERMEX and ChArMEX components supported by CNRS-INSU, IFREMER,
910 CEA, and Météo-France as part of the programme MISTRALS coordinated by INSU.
911 PEACETIME was endorsed as a process study by GEOTRACES and is a contribution to IMBER
912 and SOLAS International programs. PEACETIME cruise (<https://doi.org/10.17600/17000300>).
913 The project leading to this publication has received funding from European FEDER Fund under
914 project 1166-39417. The research of EM and MPL was supported by the Spanish Ministry of
915 Science, Innovation and Universities through project POLARIS (Grant No. PGC2018-094553B-
916 I00) and by European Union's H2020 research and innovation programme through project
917 TRIATLAS (Grant No. 817578). JD was funded by a Marie Curie Actions-International
918 Outgoing Fellowship (PIOF-GA-2013-629378).

919



920 **Acknowledgments**

921 The authors thank the captain and the crew of the RV “Pourquoi Pas ?” for their professionalism
922 and their work at sea. Céline Ridame and Kahina Djaoudi are thanked for their help during
923 sampling, Sophie Guasco and Marc Garel for their help in ectoenzymatic measurements onboard.



924 **References**

- 925 Behrenfeld, M. J., O'Malley, R. T., Siegel, D. A., McClain, C. R., Sarmiento, J. L., Feldman, G.
926 C., Milligan, A. J., Falkowski, P. G., Letelier, R. M. and Boss, E. S.: Climate-driven
927 trends in contemporary ocean productivity, *Nature*, 444(7120), 752–755, 2006.
- 928 Benner, R. and Strom, M.: A critical evaluation of the analytical blank associated with DOC
929 measurements by high-temperature catalytic oxidation, *Marine Chemistry*, 41(1), 153–
930 160, [https://doi.org/10.1016/0304-4203\(93\)90113-3](https://doi.org/10.1016/0304-4203(93)90113-3), 1993.
- 931 Bergametti, Gi., Dutot, A.-L., Buat-Ménard, P., Losno, R. and Remoudaki, E.: Seasonal
932 variability of the elemental composition of atmospheric aerosol particles over the
933 Northwestern Mediterranean, *Tellus B: Chemical and Physical Meteorology*, 41(3), 353–
934 361, <https://doi.org/10.3402/tellusb.v41i3.15092>, 1989.
- 935 Bishop, J. K. B., Davis, R. E. and Sherman, J. T.: Robotic Observations of Dust Storm
936 Enhancement of Carbon Biomass in the North Pacific, *Science*, 298(5594), 817–821,
937 <https://doi.org/10.1126/science.1074961>, 2002.
- 938 Bonnet, S. and Guieu, C.: Atmospheric forcing on the annual iron cycle in the western
939 Mediterranean Sea: A 1-year survey, *Journal of Geophysical Research: Oceans*, 111(C9),
940 <https://doi.org/10.1029/2005JC003213>, 2006.
- 941 Bonnet, S., Guieu, C., Chiaverini, J., Ras, J. and Stock, A.: Effect of atmospheric nutrients on the
942 autotrophic communities in a low nutrient, low chlorophyll system, *Limnology and*
943 *Oceanography*, 50(6), 1810–1819, <https://doi.org/10.4319/lo.2005.50.6.1810>, 2005.
- 944 Bosc, E., Bricaud, A. and Antoine, D.: Seasonal and interannual variability in algal biomass and
945 primary production in the Mediterranean Sea, as derived from 4 years of SeaWiFS
946 observations, *Global Biogeochemical Cycles*, 18(1),



- 947 <https://doi.org/10.1029/2003GB002034>, 2004.
- 948 Boscolo-Galazzo, F., Crichton, K. A., Barker, S. and Pearson, P. N.: Temperature dependency of
949 metabolic rates in the upper ocean: A positive feedback to global climate change?, *Global*
950 *and Planetary Change*, 170, 201–212, <https://doi.org/10.1016/j.gloplacha.2018.08.017>,
951 2018.
- 952 Bressac, M. and Guieu, C.: Post-depositional processes: What really happens to new atmospheric
953 iron in the ocean’s surface?, *Global Biogeochemical Cycles*, 27(3), 859–870,
954 <https://doi.org/10.1002/gbc.20076>, 2013.
- 955 Bressac, M., Guieu, C., Doxaran, D., Bourrin, F., Desboeufs, K., Leblond, N. and Ridame, C.:
956 Quantification of the lithogenic carbon pump following a simulated dust-deposition event
957 in large mesocosms, *Biogeosciences*, 11(4), 1007–1020, [https://doi.org/10.5194/bg-11-](https://doi.org/10.5194/bg-11-1007-2014)
958 1007-2014, 2014.
- 959 Brown, J. H., Gillooly, J. F., Allen, A. P., Savage, V. M. and West, G. B.: Toward a Metabolic
960 Theory of Ecology, *Ecology*, 85(7), 1771–1789, <https://doi.org/10.1890/03-9000>, 2004.
- 961 Cael, B. B. and Follows, M. J.: On the temperature dependence of oceanic export efficiency,
962 *Geophysical Research Letters*, 43(10), 5170–5175,
963 <https://doi.org/10.1002/2016GL068877>, 2016.
- 964 Cael, B. B., Bisson, K. and Follows, M. J.: How have recent temperature changes affected the
965 efficiency of ocean biological carbon export?, *Limnology and Oceanography Letters*,
966 2(4), 113–118, <https://doi.org/10.1002/lol2.10042>, 2017.
- 967 Calvo-Díaz, A., Díaz-Pérez, L., Suárez, L. Á., Morán, X. A. G., Teira, E. and Marañón, E.:
968 Decrease in the Autotrophic-to-Heterotrophic Biomass Ratio of Picoplankton in
969 Oligotrophic Marine Waters Due to Bottle Enclosure, *Appl. Environ. Microbiol.*, 77(16),



- 970 5739–5746, <https://doi.org/10.1128/AEM.00066-11>, 2011.
- 971 Chen, B. and Laws, E. A.: Is there a difference of temperature sensitivity between marine
972 phytoplankton and heterotrophs?, *Limnology and Oceanography*, 62(2), 806–817,
973 <https://doi.org/10.1002/lno.10462>, 2017.
- 974 Christaki, U., Van Wambeke, F., Lefevre, D., Lagaria, A., Prieur, L., Pujo-Pay, M.,
975 Grattepanche, J.-D., Colombet, J., Psarra, S., Dolan, J. R., Sime-Ngando, T., Conan, P.,
976 Weinbauer, M. G. and Moutin, T.: Microbial food webs and metabolic state across
977 oligotrophic waters of the Mediterranean Sea during summer, *Biogeosciences*, 8(7),
978 1839–1852, <https://doi.org/10.5194/bg-8-1839-2011>, 2011.
- 979 Desboeufs, K., Leblond, N., Wagener, T., Bon Nguyen, E. and Guieu, C.: Chemical fate and
980 settling of mineral dust in surface seawater after atmospheric deposition observed from
981 dust seeding experiments in large mesocosms, *Biogeosciences*, 11(19), 5581–5594,
982 <https://doi.org/10.5194/bg-11-5581-2014>, 2014.
- 983 Desboeufs, K., Bon Nguyen, E., Chevaillier, S., Triquet, S. and Dulac, F.: Fluxes and sources of
984 nutrient and trace metal atmospheric deposition in the Northwestern Mediterranean,
985 *Atmospheric Chemistry and Physics*, 18(19), 14477–14492, [https://doi.org/10.5194/acp-](https://doi.org/10.5194/acp-18-14477-2018)
986 [18-14477-2018](https://doi.org/10.5194/acp-18-14477-2018), 2018.
- 987 Dinasquet, J., Bigeard, E., Gazeau, F., Marañón, E., Ridame, C., Van Wambeke, F.,
988 Obernosterer, I. and Baudoux, A.-C.: Impact of dust enrichment on the microbial food
989 web under present and future conditions of pH and temperature, *Biogeosciences*
990 *Discussions*, 2021.
- 991 Dittmar, T., Cherrier, J. and Ludwichowski, K.-U.: The analysis of amino acids in seawater, in
992 *Practical Guidelines for the Analysis of Seawater*, edited by O. Wurl, pp. 67–77, CRC



- 993 Press Taylor & Francis Group, Boca Raton, FL., , 2009.
- 994 Emerson, S., Quay, P., Karl, D., Winn, C., Tupas, L. and Landry, M.: Experimental
995 determination of the organic carbon flux from open-ocean surface waters, *Nature*,
996 389(6654), 951–954, <https://doi.org/10.1038/40111>, 1997.
- 997 Engel, A.: Determination of marine gel particles, in *Practical Guidelines for the Analysis of*
998 *Seawater*, edited by O. Wurl, pp. 125–142, CRC Press Taylor & Francis Group, Boca
999 Raton, FL., , 2009.
- 1000 Engel, A. and Händel, N.: A novel protocol for determining the concentration and composition
1001 of sugars in particulate and in high molecular weight dissolved organic matter (HMW-
1002 DOM) in seawater, *Marine Chemistry*, 127(1), 180–191,
1003 <https://doi.org/10.1016/j.marchem.2011.09.004>, 2011.
- 1004 Feliú, G., Pagano, M., Hidalgo, P. and Carlotti, F.: Structure and function of epipelagic
1005 mesozooplankton and their response to dust deposition events during the spring
1006 PEACETIME cruise in the Mediterranean Sea, *Biogeosciences*, 17, 5417–5441,
1007 <https://doi.org/10.5194/bg-17-5417-2020>, 2020.
- 1008 Ferguson, R. L., Buckley, E. N. and Palumbo, A. V.: Response of marine bacterioplankton to
1009 differential filtration and confinement., *Appl. Environ. Microbiol.*, 47(1), 49–55, 1984.
- 1010 Friedlingstein, P., O’Sullivan, M., Jones, M. W., Andrew, R. M., Hauck, J., Olsen, A., Peters, G.
1011 P., Peters, W., Pongratz, J., Sitch, S., Le Quéré, C., Canadell, J. G., Ciais, P., Jackson, R.
1012 B., Alin, S., Aragão, L. E. O. C., Arneeth, A., Arora, V., Bates, N. R., Becker, M., Benoit-
1013 Cattin, A., Bittig, H. C., Bopp, L., Bultan, S., Chandra, N., Chevallier, F., Chini, L. P.,
1014 Evans, W., Florentie, L., Forster, P. M., Gasser, T., Gehlen, M., Gilfillan, D., Gkritzalis,
1015 T., Gregor, L., Gruber, N., Harris, I., Hartung, K., Haverd, V., Houghton, R. A., Ilyina,



1016 T., Jain, A. K., Joetzjer, E., Kadono, K., Kato, E., Kitidis, V., Korsbakken, J. I.,
1017 Landschützer, P., Lefèvre, N., Lenton, A., Lienert, S., Liu, Z., Lombardozzi, D., Marland,
1018 G., Metz, N., Munro, D. R., Nabel, J. E. M. S., Nakaoka, S.-I., Niwa, Y., O'Brien, K.,
1019 Ono, T., Palmer, P. I., Pierrot, D., Poulter, B., Resplandy, L., Robertson, E., Rödenbeck,
1020 C., Schwinger, J., Séférian, R., Skjelvan, I., Smith, A. J. P., Sutton, A. J., Tanhua, T.,
1021 Tans, P. P., Tian, H., Tilbrook, B., van der Werf, G., Vuichard, N., Walker, A. P.,
1022 Wanninkhof, R., Watson, A. J., Willis, D., Wiltshire, A. J., Yuan, W., Yue, X. and
1023 Zaehle, S.: Global Carbon Budget 2020, *Earth System Science Data*, 12(4), 3269–3340,
1024 <https://doi.org/10.5194/essd-12-3269-2020>, 2020.

1025 Garcia-Corral, L. S., Holding, J. M., Carrillo-de-Albornoz, P., Steckbauer, A., Pérez-Lorenzo,
1026 M., Navarro, N., Serret, P., Gasol, J. M., Morán, X. A. G., Estrada, M., Fraile-Nuez, E.,
1027 Benítez-Barrios, V., Agusti, S. and Duarte, C. M.: Temperature dependence of plankton
1028 community metabolism in the subtropical and tropical oceans, *Global Biogeochemical*
1029 *Cycles*, 31(7), 1141–1154, <https://doi.org/10.1002/2017GB005629>, 2017.

1030 Gazeau, F., Ridame, C., Van Wambeke, F., Alliouane, S., Stolpe, C., Irisson, J.-O., Marro, S.,
1031 Grisoni, J.-M., De Liège, G., Nunige, S., Djaoudi, K., Pulido-Villena, E., Dinasquet, J.,
1032 Obernosterer, I., Catala, P. and Guieu, C.: Impact of dust enrichment on Mediterranean
1033 plankton communities under present and future conditions of pH and temperature: an
1034 overview, *Biogeosciences Discussions*, <https://doi.org/10.5194/bg-2020-202>, 2020.

1035 Gillikin, D. P. and Bouillon, S.: Determination of $\delta^{18}\text{O}$ of water and $\delta^{13}\text{C}$ of dissolved inorganic
1036 carbon using a simple modification of an elemental analyser-isotope ratio mass
1037 spectrometer: an evaluation, *Rapid Communications in Mass Spectrometry*, 21(8), 1475–
1038 1478, <https://doi.org/10.1002/rcm.2968>, 2007.



- 1039 Gillooly, J. F., Brown, J. H., West, G. B., Savage, V. M. and Charnov, E. L.: Effects of Size and
1040 Temperature on Metabolic Rate, *Science*, 293(5538), 2248–2251,
1041 <https://doi.org/10.1126/science.1061967>, 2001.
- 1042 del Giorgio, P. and Williams, P.: Respiration in Aquatic Ecosystems, Oxford University Press.
1043 [https://oxford.universitypressscholarship.com/view/10.1093/acprof:oso/9780198527084.](https://oxford.universitypressscholarship.com/view/10.1093/acprof:oso/9780198527084.001.0001/acprof-9780198527084)
1044 001.0001/acprof-9780198527084, last access: 22 January 2021, 2005.
- 1045 Guieu, C. and Ridame, C.: Impact of atmospheric deposition on marine chemistry and
1046 biogeochemistry, in *Atmospheric Chemistry in the Mediterranean Region: Comprehensive Diagnosis and Impacts*, edited by F. Dulac, S. Sauvage, and E. Hamonou,
1047 Springer, Cham, Switzerland, , 2020.
- 1049 Guieu, C., Loye-Pilot, M. D., Benyahya, L. and Dufour, A.: Spatial variability of atmospheric
1050 fluxes of metals (Al, Fe, Cd, Zn and Pb) and phosphorus over the whole Mediterranean
1051 from a one-year monitoring experiment: Biogeochemical implications, *Marine*
1052 *Chemistry*, 120(1–4), 164–178, <https://doi.org/10.1016/j.marchem.2009.02.004>, 2010.
- 1053 Guieu, C., Ridame, C., Pulido-Villena, E., Bressac, M., Desboeufs, K. and Dulac, F.: Impact of
1054 dust deposition on carbon budget: a tentative assessment from a mesocosm approach,
1055 *Biogeosciences*, 11(19), 5621–5635, 2014a.
- 1056 Guieu, C., Aumont, O., Paytan, A., Bopp, L., Law, C. S., Mahowald, N., Achterberg, E. P.,
1057 Marañón, E., Salihoglu, B., Crise, A., Wagener, T., Herut, B., Desboeufs, K., Kanakidou,
1058 M., Olgun, N., Peters, F., Pulido-Villena, E., Tovar-Sanchez, A. and Völker, C.: The
1059 significance of the episodic nature of atmospheric deposition to Low Nutrient Low
1060 Chlorophyll regions, *Global Biogeochemical Cycles*, 28(11), 1179–1198,
1061 <https://doi.org/10.1002/2014GB004852>, 2014b.



- 1062 Guieu, C., D’Ortenzio, F., Dulac, F., Taillandier, V., Doglioli, A., Petrenko, A., Barrillon, S.,
1063 Mallet, M., Nabat, P. and Desboeufs, K.: Process studies at the air-sea interface after
1064 atmospheric deposition in the Mediterranean Sea: objectives and strategy of the
1065 PEACETIME oceanographic campaign (May–June 2017), *Biogeosciences*, 2020(17),
1066 5563–5585, <https://doi.org/10.5194/bg-17-5563-2020>, 2020.
- 1067 Hein, M. and Sand-Jensen, K.: CO₂ increases oceanic primary production, *Nature*, 388(6642),
1068 526–527, 1997.
- 1069 Herut, B., Zohary, T., Krom, M. D., Mantoura, R. F. C., Pitta, P., Psarra, S., Rassoulzadegan, F.,
1070 Tanaka, T. and Frede Thingstad, T.: Response of East Mediterranean surface water to
1071 Saharan dust: On-board microcosm experiment and field observations, *Deep Sea*
1072 *Research Part II: Topical Studies in Oceanography*, 52(22), 3024–3040,
1073 <https://doi.org/10.1016/j.dsr2.2005.09.003>, 2005.
- 1074 Herut, B., Rahav, E., Tsagaraki, T. M., Giannakourou, A., Tsiola, A., Psarra, S., Lagaria, A.,
1075 Papageorgiou, N., Mihalopoulos, N., Theodosi, C. N., Violaki, K., Stathopoulou, E.,
1076 Scoullou, M., Krom, M. D., Stockdale, A., Shi, Z., Berman-Frank, I., Meador, T. B.,
1077 Tanaka, T. and Paraskevi, P.: The Potential Impact of Saharan Dust and Polluted
1078 Aerosols on Microbial Populations in the East Mediterranean Sea, an Overview of a
1079 Mesocosm Experimental Approach, *Front. Mar. Sci.*, 3,
1080 <https://doi.org/10.3389/fmars.2016.00226>, 2016.
- 1081 Hoppe, H.-G.: Significance of exoenzymatic activities in the ecology of brackish water:
1082 measurements by means of methylumbelliferyl-substrates, *Marine Ecology Progress*
1083 *Series*, 11(3), 299–308, 1983.
- 1084 IPCC: *Climate Change, The Physical Science Basis.*, 2013.



- 1085 Irwin, A. J. and Oliver, M. J.: Are ocean deserts getting larger?, *Geophysical Research Letters*,
1086 36, <https://doi.org/10.1029/2009gl039883>, 2009.
- 1087 Jickells, T. and Moore, C. M.: The Importance of Atmospheric Deposition for Ocean
1088 Productivity, *Annual Review of Ecology, Evolution, and Systematics*, 46(1), 481–501,
1089 <https://doi.org/10.1146/annurev-ecolsys-112414-054118>, 2015.
- 1090 Kirchman, D. L., Kemp, P., Sherr, B., Sherr, E. and Cole, J.: Leucine Incorporation as a Measure
1091 of Biomass Production by Heterotrophic Bacteria, in *Handbook of Methods in Aquatic*
1092 *Microbial Ecology*, pp. 509–512, CRC Press, <https://doi.org/10.1201/9780203752746-59>,
1093 , 1993.
- 1094 Knap, A., Michaels, A., Close, A., Ducklow, H. and Dickson, A.: Protocols for the Joint Global
1095 Ocean Flux Study (JGOFS) Core Measurements, UNESCO 1994., 1996.
- 1096 Kouvarakis, G., Mihalopoulos, N., Tselepides, A. and Stavrakakis, S.: On the importance of
1097 atmospheric inputs of inorganic nitrogen species on the productivity of the Eastern
1098 Mediterranean Sea, *Global Biogeochemical Cycles*, 15(4), 805–817,
1099 <https://doi.org/10.1029/2001GB001399>, 2001.
- 1100 Kroeker, K. J., Kordas, R. L., Crim, R., Hendriks, I. E., Ramajo, L., Singh, G. S., Duarte, C. M.
1101 and Gattuso, J. P.: Impacts of ocean acidification on marine organisms: quantifying
1102 sensitivities and interaction with warming, *Global Change Biology*, 19(6), 1884–1896,
1103 <https://doi.org/10.1111/gcb.12179>, 2013.
- 1104 Langer, G., Nehrke, G., Probert, I., Ly, J. and Ziveri, P.: Strain-specific responses of *Emiliania*
1105 *huxleyi* to changing seawater carbonate chemistry, *Biogeosciences*, 6(11), 2637–2646,
1106 <https://doi.org/10.5194/bg-6-2637-2009>, 2009.
- 1107 Laurent, B., Audoux, T., Bibi, M., Dulac, F. and Bergametti, G.: Mass deposition in the



- 1108 Mediterranean region, in *Atmospheric Chemistry in the Mediterranean Region:*
1109 *Comprehensive Diagnosis and Impacts*, edited by F. Dulac, S. Sauvage, and E. Hamonou,
1110 Springer, Cham, Switzerland, , 2021.
- 1111 Lazzari, P., Solidoro, C., Salon, S. and Bolzon, G.: Spatial variability of phosphate and nitrate in
1112 the Mediterranean Sea: A modeling approach, *Deep Sea Research Part I: Oceanographic*
1113 *Research Papers*, 108, 39–52, <https://doi.org/10.1016/j.dsr.2015.12.006>, 2016.
- 1114 Lekunberri, I., Lefort, T., Romero, E., Vázquez-Domínguez, E., Romera-Castillo, C., Marrasé,
1115 C., Peters, F., Weinbauer, M. and Gasol, J. M.: Effects of a dust deposition event on
1116 coastal marine microbial abundance and activity, bacterial community structure and
1117 ecosystem function, *J Plankton Res*, 32(4), 381–396,
1118 <https://doi.org/10.1093/plankt/fbp137>, 2010.
- 1119 Lemée, R., Rochelle-Newall, E., Van Wambeke, F., Pizay, M., Rinaldi, P. and Gattuso, J.:
1120 Seasonal variation of bacterial production, respiration and growth efficiency in the open
1121 NW Mediterranean Sea, *Aquat. Microb. Ecol.*, 29, 227–237,
1122 <https://doi.org/10.3354/ame029227>, 2002.
- 1123 Lewandowska, A. M., Boyce, D. G., Hofmann, M., Matthiessen, B., Sommer, U. and Worm, B.:
1124 Effects of sea surface warming on marine plankton, *Ecology Letters*, 17(5), 614–623,
1125 <https://doi.org/10.1111/ele.12265>, 2014.
- 1126 Lindroth, P. and Mopper, K.: High performance liquid chromatographic determination of
1127 subpicomole amounts of amino acids by precolumn fluorescence derivatization with o-
1128 phthaldialdehyde, *Anal. Chem.*, 51(11), 1667–1674,
1129 <https://doi.org/10.1021/ac50047a019>, 1979.
- 1130 Longhurst, A., Sathyendranath, S., Platt, T. and Caverhill, C.: An estimate of global primary



- 1131 production in the ocean from satellite radiometer data, *Journal of Plankton Research*,
1132 17(6), 1245–1271, <https://doi.org/10.1093/plankt/17.6.1245>, 1995.
- 1133 Lopez-Urrutia, A. and Moran, X. A. G.: Resource limitation of bacterial production distorts the
1134 temperature dependence of oceanic carbon cycling, *Ecology*, 88(4), 817–822, 2007.
- 1135 Louis, J., Pedrotti, M. L., Gazeau, F. and Guieu, C.: Experimental evidence of formation of
1136 transparent exopolymer particles (TEP) and POC export provoked by dust addition under
1137 current and high $p\text{CO}_2$ conditions, *PLOS ONE*, 12(2), e0171980,
1138 <https://doi.org/10.1371/journal.pone.0171980>, 2017.
- 1139 Lojze-Pilot, M. D. and Martin, J. M.: Saharan Dust Input to the Western Mediterranean: An
1140 Eleven Years Record in Corsica, in *The Impact of Desert Dust Across the Mediterranean*,
1141 edited by S. Guerzoni and R. Chester, pp. 191–199, Springer Netherlands, Dordrecht,
1142 https://doi.org/10.1007/978-94-017-3354-0_18, , 1996.
- 1143 Mackey, K., Morris, J. J., Morel, F. and Kranz, S.: Response of photosynthesis to ocean
1144 acidification, *Oceanography*, 25(2), 74–91, <https://doi.org/10.5670/oceanog.2015.33>,
1145 2015.
- 1146 Marañón, E., Fernández, A., Mouriño-Carballido, B., Martínez-García, S., Teira, E., Cermeño,
1147 P., Chouciño, P., Huete-Ortega, M., Fernández, E., Calvo-Díaz, A., Morán, X. A. G.,
1148 Bode, A., Moreno-Ostos, E., Varela, M. M., Patey, M. D. and Achterberg, E. P.: Degree
1149 of oligotrophy controls the response of microbial plankton to Saharan dust, *Limnology
1150 and Oceanography*, 55(6), 2339–2352, <https://doi.org/10.4319/lo.2010.55.6.2339>, 2010.
- 1151 Marañón, E., Lorenzo, M. P., Cermeño, P. and Mouriño-Carballido, B.: Nutrient limitation
1152 suppresses the temperature dependence of phytoplankton metabolic rates, *The ISME
1153 Journal*, 12(7), 1836–1845, <https://doi.org/10.1038/s41396-018-0105-1>, 2018.



- 1154 Marañón, E., Van Wambeke, F., Uitz, J., Boss, E. S., Pérez-Lorenzo, M., Dinasquet, J.,
1155 Haëntjens, N., Dimier, C. and Taillandier, V.: Deep maxima of phytoplankton biomass,
1156 primary production and bacterial production in the Mediterranean Sea during late spring,
1157 Biogeosciences Discussions, 1–28, <https://doi.org/10.5194/bg-2020-261>, 2020.
- 1158 Mari, X.: Carbon content and C:N ratio of transparent exopolymeric particles (TEP) produced by
1159 bubbling exudates of diatoms, Marine Ecology Progress Series, 183, 59–71,
1160 <https://doi.org/10.3354/meps183059>, 1999.
- 1161 Markaki, Z., Oikonomou, K., Kocak, M., Kouvarakis, G., Chaniotaki, A., Kubilay, N. and
1162 Mihalopoulos, N.: Atmospheric deposition of inorganic phosphorus in the Levantine
1163 Basin, eastern Mediterranean: Spatial and temporal variability and its role in seawater
1164 productivity, Limnology and Oceanography, 48(4), 1557–1568,
1165 <https://doi.org/10.4319/lo.2003.48.4.1557>, 2003.
- 1166 Maugendre, L., Gattuso, J.-P., Louis, J., de Kluijver, A., Marro, S., Soetaert, K. and Gazeau, F.:
1167 Effect of ocean warming and acidification on a plankton community in the NW
1168 Mediterranean Sea, ICES Journal of Marine Science: Journal du Conseil, 72(6), 1744–
1169 1755, <https://doi.org/10.1093/icesjms/fsu161>, 2015.
- 1170 Maugendre, L., Gattuso, J.-P., Poulton, A. J., Dellisanti, W., Gaubert, M., Guieu, C. and Gazeau,
1171 F.: No detectable effect of ocean acidification on plankton metabolism in the NW
1172 oligotrophic Mediterranean Sea: Results from two mesocosm studies, Estuarine, Coastal
1173 and Shelf Science, 186, 89–99, <https://doi.org/10.1016/j.ecss.2015.03.009>, 2017a.
- 1174 Maugendre, L., Guieu, C., Gattuso, J.-P. and Gazeau, F.: Ocean acidification in the
1175 Mediterranean Sea: Pelagic mesocosm experiments. A synthesis, Estuarine, Coastal and
1176 Shelf Science, 186, 1–10, <https://doi.org/10.1016/j.ecss.2017.01.006>, 2017b.



- 1177 Mercado, J. M., Sobrino, C., Neale, P. J., Segovia, M., Reul, A., Amorim, A. L., Carrillo, P.,
1178 Claquin, P., Cabrerizo, M. J., León, P., Lorenzo, M. R., Medina-Sánchez, J. M.,
1179 Montecino, V., Napoleon, C., Prasil, O., Putzeys, S., Salles, S. and Yebra, L.: Effect of
1180 CO₂, nutrients and light on coastal plankton. II. Metabolic rates, *Aquatic Biology*, 22,
1181 43–57, <https://doi.org/10.3354/ab00606>, 2014.
- 1182 Mills, M. M., Moore, C. M., Langlois, R., Milne, A., Achterberg, E., Nachtigall, K., Lochte, K.,
1183 Geider, R. J. and La, R. J.: Nitrogen and phosphorus co-limitation of bacterial
1184 productivity and growth in the oligotrophic subtropical North Atlantic, *Limnology and*
1185 *Oceanography*, 53(2), 824–834, <https://doi.org/10.4319/lo.2008.53.2.0824>, 2008.
- 1186 Mosseri, J., Quéguiner, B., Rimmelin, P., Leblond, N. and Guieu, C.: Silica fluxes in the
1187 northeast Atlantic frontal zone of Mode Water formation (38°–45°N, 16°–22°W) in
1188 2001–2002, *Journal of Geophysical Research: Oceans*, 110(C7),
1189 <https://doi.org/10.1029/2004JC002615>, 2005.
- 1190 Moulin, C. and Chiapello, I.: Impact of human-induced desertification on the intensification of
1191 Sahel dust emission and export over the last decades, *Geophysical Research Letters*,
1192 33(18), <https://doi.org/10.1029/2006GL025923>, 2006.
- 1193 Moutin, T. and Raimbault, P.: Primary production, carbon export and nutrients availability in
1194 western and eastern Mediterranean Sea in early summer 1996 (MINOS cruise), *Journal of*
1195 *Marine Systems*, 33–34, 273–288, [https://doi.org/10.1016/S0924-7963\(02\)00062-3](https://doi.org/10.1016/S0924-7963(02)00062-3),
1196 2002.
- 1197 Moutin, T., Thingstad, T. F., Wambeke, F. V., Marie, D., Slawyk, G., Raimbault, P. and
1198 Claustre, H.: Does competition for nanomolar phosphate supply explain the
1199 predominance of the cyanobacterium *Synechococcus*?, *Limnology and Oceanography*,



- 1200 47(5), 1562–1567, <https://doi.org/10.4319/lo.2002.47.5.1562>, 2002.
- 1201 Müren, U., Berglund, J., Samuelsson, K. and Andersson, A.: Potential Effects of Elevated Sea-
1202 Water Temperature on Pelagic Food Webs, *Hydrobiologia*, 545(1), 153–166,
1203 <https://doi.org/10.1007/s10750-005-2742-4>, 2005.
- 1204 Passow, U. and Carlson, C. A.: The biological pump in a high CO₂ world, *Marine Ecology*
1205 *Progress Series*, 470, 249–271, 2012.
- 1206 Polovina, J. J., Howell, E. A. and Abecassis, M.: Ocean’s least productive waters are expanding,
1207 *Geophysical Research Letters*, 35(3), <https://doi.org/10.1029/2007gl031745>, 2008.
- 1208 Pulido-Villena, E., Wagener, T. and Guieu, C.: Bacterial response to dust pulses in the western
1209 Mediterranean: Implications for carbon cycling in the oligotrophic ocean, *Global*
1210 *Biogeochemical Cycles*, 22(1), <https://doi.org/10.1029/2007gb003091>, 2008.
- 1211 Pulido-Villena, E., Baudoux, A.-C., Obernosterer, I., Landa, M., Caparros, J., Catala, P.,
1212 Georges, C., Harmand, J. and Guieu, C.: Microbial food web dynamics in response to a
1213 Saharan dust event: results from a mesocosm study in the oligotrophic Mediterranean
1214 Sea, *Biogeosciences*, 11(19), 5607–5619, 2014.
- 1215 Regaudie-de-Gioux, A. and Duarte, C. M.: Temperature dependence of planktonic metabolism in
1216 the ocean, *Global Biogeochemical Cycles*, 26(1), <https://doi.org/10.1029/2010GB003907>,
1217 2012.
- 1218 Regaudie-de-Gioux, A., Vaquer-Sunyer, R. and Duarte, C. M.: Patterns in planktonic
1219 metabolism in the Mediterranean Sea, *Biogeosciences*, 6(12), 3081–3089,
1220 <https://doi.org/10.5194/bg-6-3081-2009>, 2009.
- 1221 Ridame, C. and Guieu, C.: Saharan input of phosphate to the oligotrophic water of the open
1222 western Mediterranean Sea, *Limnology and Oceanography*, 47(3), 856–869, 2002.



- 1223 Riebesell, U., Schulz, K. G., Bellerby, R. G. J., Botros, M., Fritsche, P., Meyerhofer, M., Neill,
1224 C., Nondal, G., Oschlies, A., Wohlers, J. and Zollner, E.: Enhanced biological carbon
1225 consumption in a high CO₂ ocean, *Nature*, 450(7169), 545-U10, 2007.
- 1226 Smith, D. C. and Azam, F.: A simple, economical method for measuring bacterial protein
1227 synthesis rates in seawater using 3H-leucine, *Marine Microbial Food Webs*, 6(2), 107–
1228 114, 1992.
- 1229 Tanaka, T., Thingstad, T. F., Christaki, U., Colombet, J., Cornet-Barthaux, V., Courties, C.,
1230 Grattepanche, J.-D., Lagaria, A., Nedoma, J., Oriol, L., Psarra, S., Pujo-Pay, M. and
1231 Wambeke, F. V.: Lack of P-limitation of phytoplankton and heterotrophic prokaryotes in
1232 surface waters of three anticyclonic eddies in the stratified Mediterranean Sea,
1233 *Biogeosciences*, 8(2), 525–538, <https://doi.org/10.5194/bg-8-525-2011>, 2011.
- 1234 Ternon, E., Guieu, C., Loÿe-Pilot, M.-D., Leblond, N., Bosc, E., Gasser, B., Miquel, J.-C. and
1235 Martín, J.: The impact of Saharan dust on the particulate export in the water column of
1236 the North Western Mediterranean Sea, *Biogeosciences*, 7(3), 809–826,
1237 <https://doi.org/10.5194/bg-7-809-2010>, 2010.
- 1238 Thingstad, T. F., Krom, M. D., Mantoura, R. F. C., Flaten, G. a. F., Groom, S., Herut, B., Kress,
1239 N., Law, C. S., Pasternak, A., Pitta, P., Psarra, S., Rassoulzadegan, F., Tanaka, T.,
1240 Tselepidis, A., Wassmann, P., Woodward, E. M. S., Riser, C. W., Zodiatis, G. and
1241 Zohary, T.: Nature of Phosphorus Limitation in the Ultraoligotrophic Eastern
1242 Mediterranean, *Science*, 309(5737), 1068–1071, <https://doi.org/10.1126/science.1112632>,
1243 2005.
- 1244 Van Wambeke, F., Taillandier, V., Deboeufs, K., Pulido-Villena, E., Dinasquet, J., Engel, A.,
1245 Marañón, E., Ridame, C. and Guieu, C.: Influence of atmospheric deposition on



- 1246 biogeochemical cycles in an oligotrophic ocean system, *Biogeosciences Discussions*, 1–
1247 51, <https://doi.org/10.5194/bg-2020-411>, 2020a.
- 1248 Van Wambeke, F., Pulido, E., Dinasquet, J., Djaoudi, K., Engel, A., Garel, M., Guasco, S.,
1249 Nunige, S., Taillandier, V., Zäncker, B. and Tamburini, C.: Spatial patterns of biphasic
1250 ectoenzymatic kinetics related to biogeochemical properties in the Mediterranean Sea,
1251 *Biogeosciences Discussions*, 1–38, <https://doi.org/10.5194/bg-2020-253>, 2020b.
- 1252 Wang, Q., Lyu, Z., Omar, S., Cornell, S., Yang, Z. and Montagnes, D. J. S.: Predicting
1253 temperature impacts on aquatic productivity: Questioning the metabolic theory of
1254 ecology’s “canonical” activation energies, *Limnology and Oceanography*, 64(3), 1172–
1255 1185, <https://doi.org/10.1002/lno.11105>, 2019.
- 1256 Zobell, C. E. and Anderson, D. Q.: Observations on the multiplication of bacteria in different
1257 volumes of stored sea water and the influence of oxygen tension and solid surfaces, *The*
1258 *Biological Bulletin*, 71(2), 324–342, <https://doi.org/10.2307/1537438>, 1936.



Tables

- 1259
- 1260 Table 1. Initial chemical and biological stocks as measured while filling the tanks (initial conditions in pumped surface water;
- 1261 sampling time: t-12h). NO_x: nitrate + nitrite, DIP: dissolved inorganic phosphorus, Si(OH)₄: silicate, POC: particulate organic carbon,
- 1262 DOC: dissolved organic carbon, TEP: transparent exopolymer particles, TChl_a: total chlorophyll *a*. Values shown for ¹⁴C
- 1263 incorporation rates, percentages of extracellular release (%PER) as well as for net community production (NCP), community
- 1264 respiration (CR) and gross primary production (GPP) were estimated from samples taken at t0 in the control tanks. For heterotrophic
- 1265 bacterial production (BP), rates were estimated from seawater sampled at t-12h.

Sampling station	TYR	ION	FAST
Coordinates (decimal)	39.34 N, 12.60 E	35.49 N, 19.78 E	37.95 N, 2.90 N
Bottom depth (m)	3395	3054	2775
Day and time of pumping (local time)	17/05/2017 17:00	25/05/2017 17:00	02/06/2017 21:00
Temperature (°C)	20.6	21.2	21.5
Salinity	37.96	39.02	37.07
Stocks			
NO _x (nmol L ⁻¹)	14.0	18.0	59.0
DIP (nmol L ⁻¹)	17.1	6.5	12.9
Si(OH) ₄ (μmol L ⁻¹)	1.0	0.96	0.64



POC ($\mu\text{mol L}^{-1}$)	12.9	8.5	6.0
DOC ($\mu\text{mol L}^{-1}$)	72.2	70.2	69.6
TEP ($\times 10^6 \text{ L}^{-1}$)	6.8	3.8	3.7
TChl <i>a</i> ($\mu\text{g L}^{-1}$)	0.063	0.066	0.072
Heterotrophic prokaryotes abundance ($\times 10^5 \text{ cell mL}^{-1}$)	4.79	2.14	6.15
Processes			
^{14}C -based total particulate production ($\mu\text{g C L}^{-1} \text{ h}^{-1}$)	0.08 ± 0.03	0.14 ± 0.04	0.15 ± 0.04
^{14}C -based $> 2 \mu\text{m}$ particulate production ($\mu\text{g C L}^{-1} \text{ h}^{-1}$)	0.07 ± 0.02	0.11 ± 0.02	0.11 ± 0.02
^{14}C -based $< 2 \mu\text{m}$ particulate production ($\mu\text{g C L}^{-1} \text{ h}^{-1}$)	0.01 ± 0.01	0.04 ± 0.02	0.05 ± 0.01
%PER	60 ± 20	45 ± 3	32 ± 23
NCP ($\mu\text{mol O}_2 \text{ L}^{-1} \text{ d}^{-1}$)	-1.9 ± 0.3	-0.2 ± 0.2	-0.8 ± 0.9
CR ($\mu\text{mol O}_2 \text{ L}^{-1} \text{ d}^{-1}$)	-2.6 ± 0.1	-1.2 ± 0.5	-1.9 ± 1.6
GPP ($\mu\text{mol O}_2 \text{ L}^{-1} \text{ d}^{-1}$)	0.7 ± 0.4	1.1 ± 0.3	1.1 ± 0.7
BP ($\text{ng C L}^{-1} \text{ h}^{-1}$)	11.6	15.2	34.6



1267 Table 2. Heterotrophic bacterial production (BP) growth rates (μ_{BP} in h^{-1}) estimated from the
1268 exponential phase of BP growth, observable from at least four sampling points, between t_0 and
1269 t_{12h} , during the three experiments (TYR, ION and FAST) in the six tanks (controls: C1, C2; dust
1270 addition under present conditions of temperature and pH: D1, D2; dust addition under future
1271 conditions of temperature and pH: G1 and G2). Values \pm SE are shown.

	μ_{BP}		
	TYR	ION	FAST
C1	0.076 ± 0.025	0.042 ± 0.007	0.020 ± 0.003
C2	0.066 ± 0.018	0.041 ± 0.005	0.026 ± 0.004
D1	0.117 ± 0.008	0.095 ± 0.020	0.089 ± 0.014
D2	0.194 ± 0.020	0.145 ± 0.007	0.090 ± 0.007
G1	0.164 ± 0.020	0.126 ± 0.011	0.124 ± 0.005
G2	0.150 ± 0.003	0.137 ± 0.033	0.163 ± 0.014

1272



1273 Table 3. Estimated bacterial growth efficiency (BGE in %) during the course of the three
1274 experiments (TYR, ION and FAST) in the six tanks (controls: C1, C2; dust addition under
1275 present conditions of temperature and pH: D1, D2; dust addition under future conditions of
1276 temperature and pH: G1 and G2). BGE was calculated based on integrated heterotrophic
1277 bacterial production (BP) and community respiration (CR) rates by applying a bacterial
1278 respiration to CR ratio of 0.7 and a respiratory quotient of 0.8 (see Material and Methods).

Bacterial growth efficiency (BGE)			
	TYR	ION	FAST
C1	11.1	9.8	15.4
C2	11.7	14.5	22.0
D1	31.8	21.0	17.3
D2	32.3	30.6	19.9
G1	39.3	35.2	37.6
G2	32.5	34.8	38.1

1279

1280



1281 **Figure caption**

1282 Fig. 1. Map showing the sampling stations in the Mediterranean Sea along the transect performed
1283 onboard the R/V “Pourquoi Pas ?” during the PEACETIME cruise.

1284 Fig. 2. Dissolved organic carbon (DOC) concentrations and ratio between total hydrolysable
1285 amino acids (TAA) and DOC concentrations measured in the six tanks (controls: C1, C2; dust
1286 addition under present conditions of temperature and pH: D1, D2; dust addition under future
1287 conditions of temperature and pH: G1 and G2) during the three experiments (TYR, ION and
1288 FAST). The dashed vertical line indicates the time of seeding (after t_0).

1289 Fig. 3. Particulate organic carbon (POC) concentrations and transparent exopolymer particle
1290 carbon content (TEP-C) measured in the six tanks (controls: C1, C2; dust addition under present
1291 conditions of temperature and pH: D1, D2; dust addition under future conditions of temperature
1292 and pH: G1 and G2) during the three experiments (TYR, ION and FAST). The dashed vertical
1293 line indicates the time of seeding (after t_0).

1294 Fig. 4. ^{14}C -based production rates ($< 2 \mu\text{m}$ and $> 2 \mu\text{m}$ size fractions, total particulate) estimated
1295 from 8 h incubations on samples taken in the six tanks (controls: C1, C2; dust addition under
1296 present conditions of temperature and pH: D1, D2; dust addition under future conditions of
1297 temperature and pH: G1 and G2) during the three experiments (TYR, ION and FAST). The
1298 percentage of extracellular release (%PER) is also shown.

1299 Fig. 5. Incorporation of ^{13}C into particulate organic carbon ($\delta^{13}\text{C}$ -POC) in the six tanks (controls:
1300 C1, C2; dust addition under present conditions of temperature and pH: D1, D2; dust addition



1301 under future conditions of temperature and pH: G1 and G2) during the three experiments (TYR,
1302 ION and FAST). The dashed vertical line indicates the time of seeding (after t_0).

1303 Fig. 6. Net community production (NCP), community respiration (CR) and gross primary
1304 production (GPP) rates estimated using the oxygen light-dark method (24 h incubations) on
1305 samples taken in the six tanks (C1, C2, D1, D2, G1 and G2) during the three experiments (TYR,
1306 ION and FAST).

1307 Fig. 7. Heterotrophic bacterial production rates (BP) and cell-specific maximum hydrolysis
1308 velocity (V_m) of the alkaline phosphatase (both over 1-2 h incubations) on samples taken in the
1309 six tanks (C1, C2, D1, D2, G1 and G2) during the three experiments (TYR, ION and FAST).

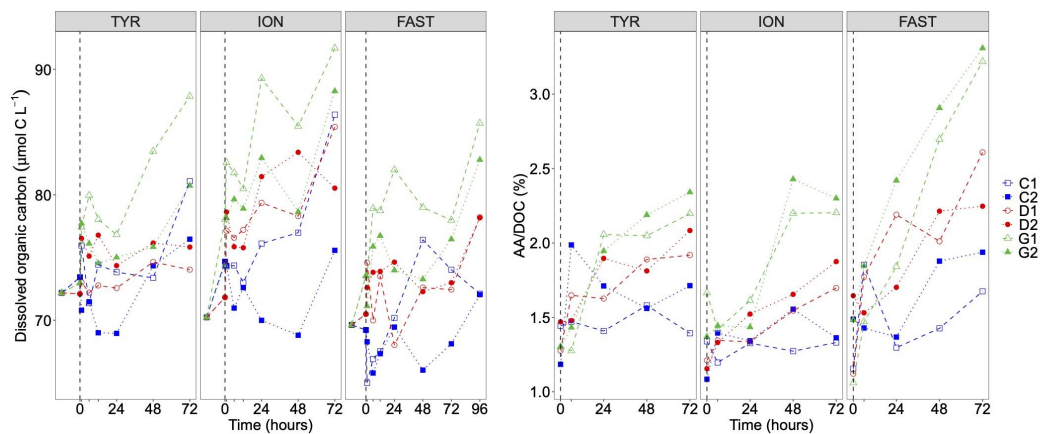
1310 Fig. 8. Total mass and organic matter fluxes measured in the sediment traps at the end of the
1311 three experiments (TYR, ION and FAST) in the six tanks (C1, C2, D1, D2, G1 and G2).

1312 Fig. 9. Relative difference (%) between integrated rates measured in tanks D (D1, D2; dust
1313 addition under present conditions of temperature and pH) and G (G1, G2; dust addition under
1314 future conditions of temperature and pH) as compared to the controls (C1, C2) during the three
1315 experiments (TYR, ION and FAST). Vertical boxes represent the range observed between the
1316 two replicates per treatment.



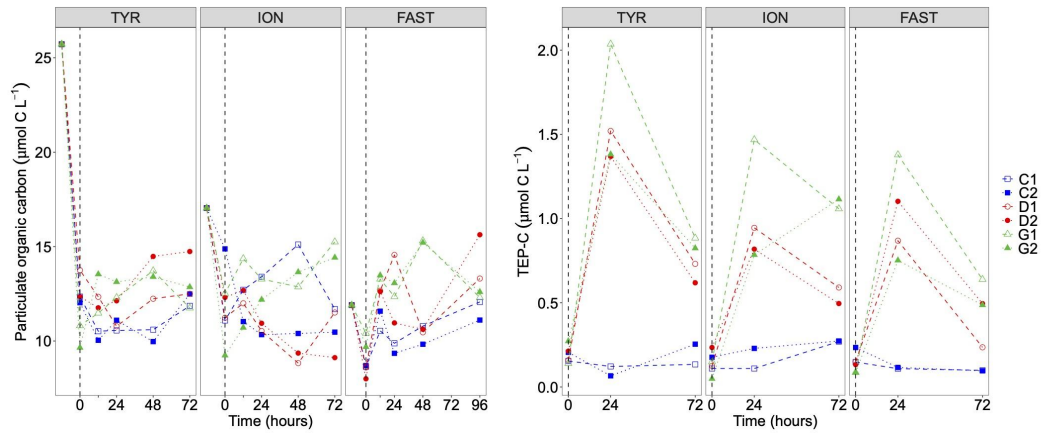
1317

1318 Fig. 1



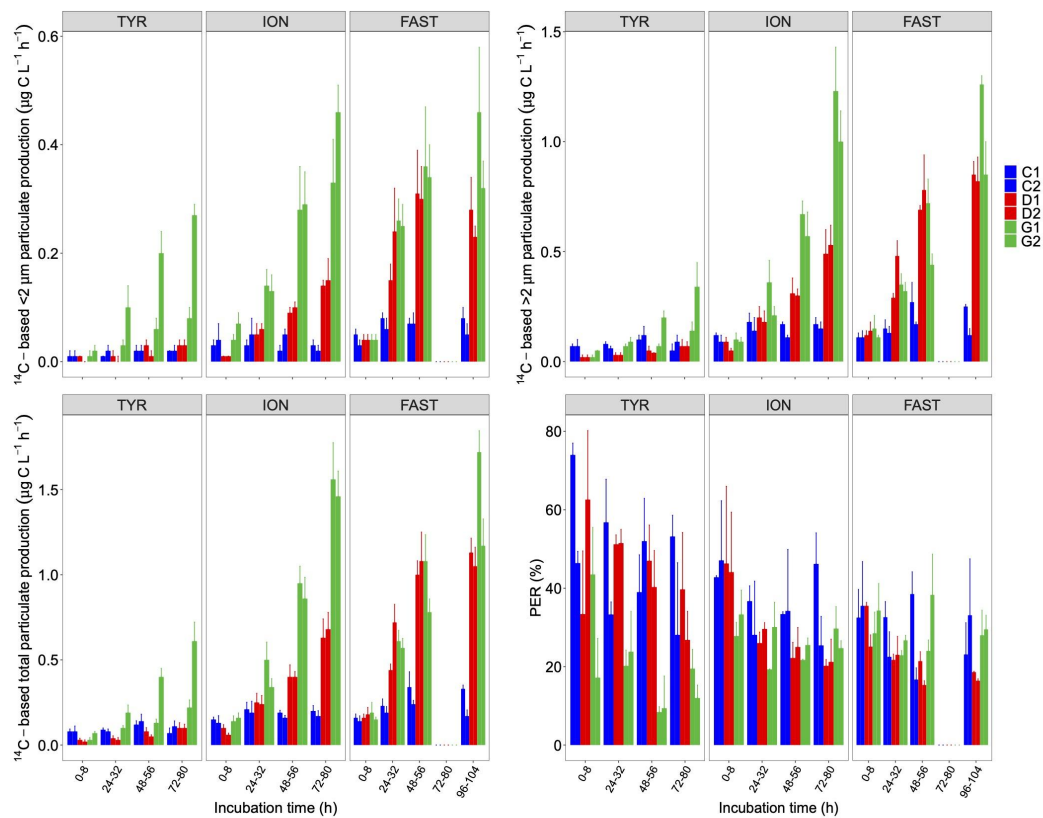
1319

1320 Fig. 2



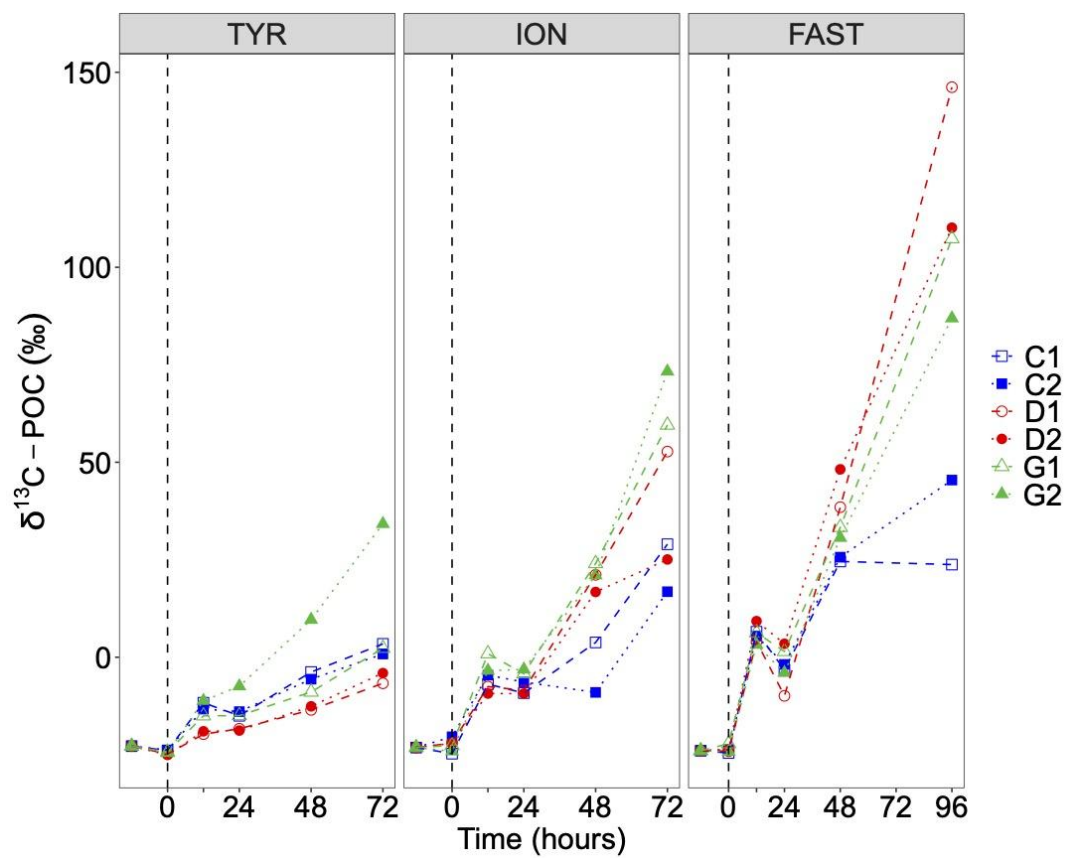
1321

1322 Fig. 3



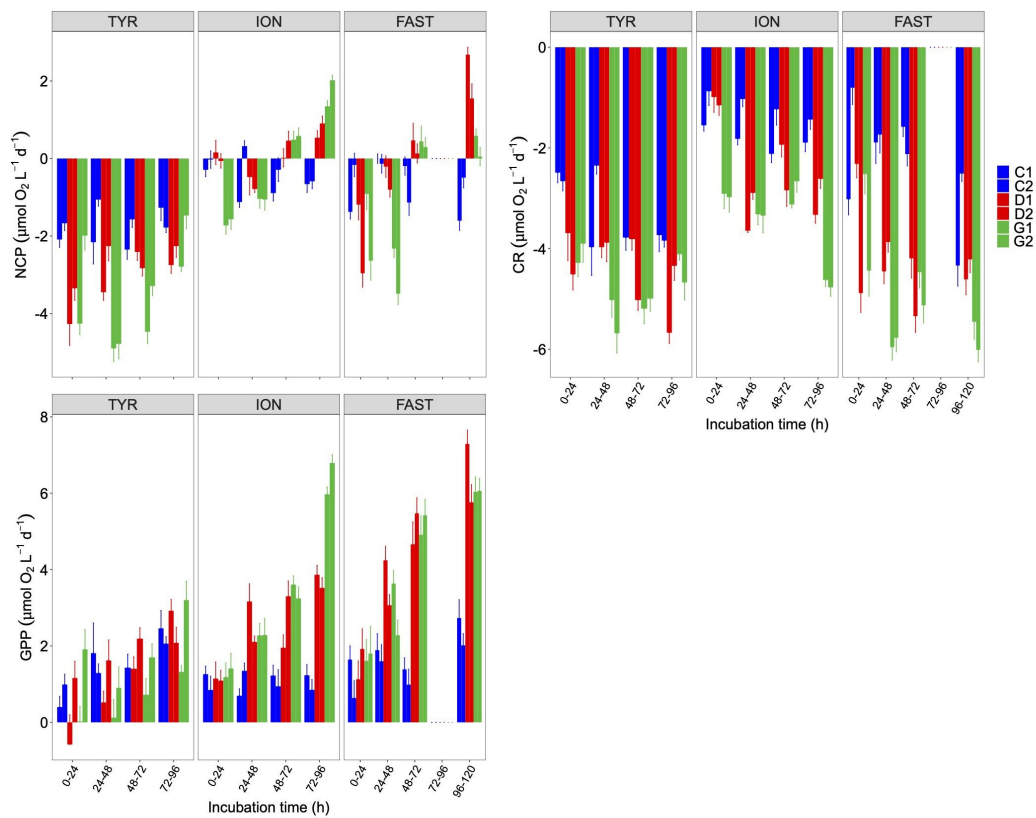
1323

1324 Fig. 4



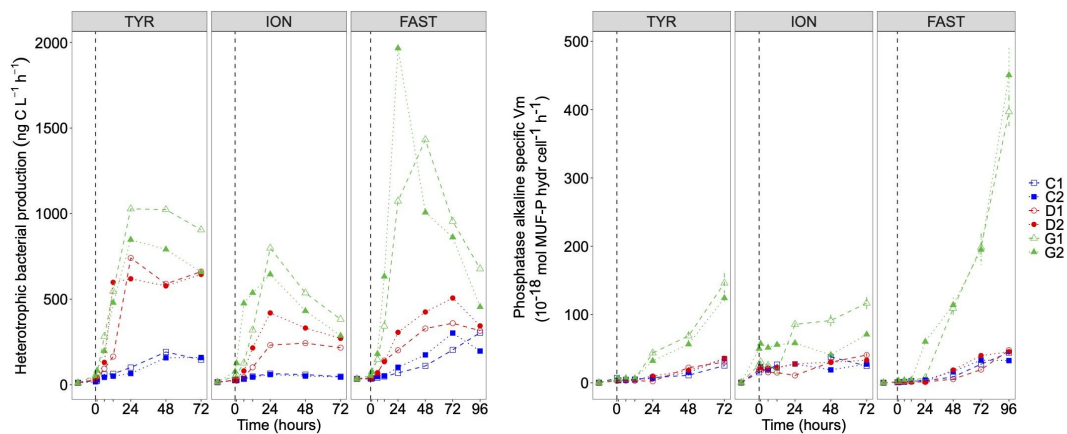
1325

1326 Fig. 5



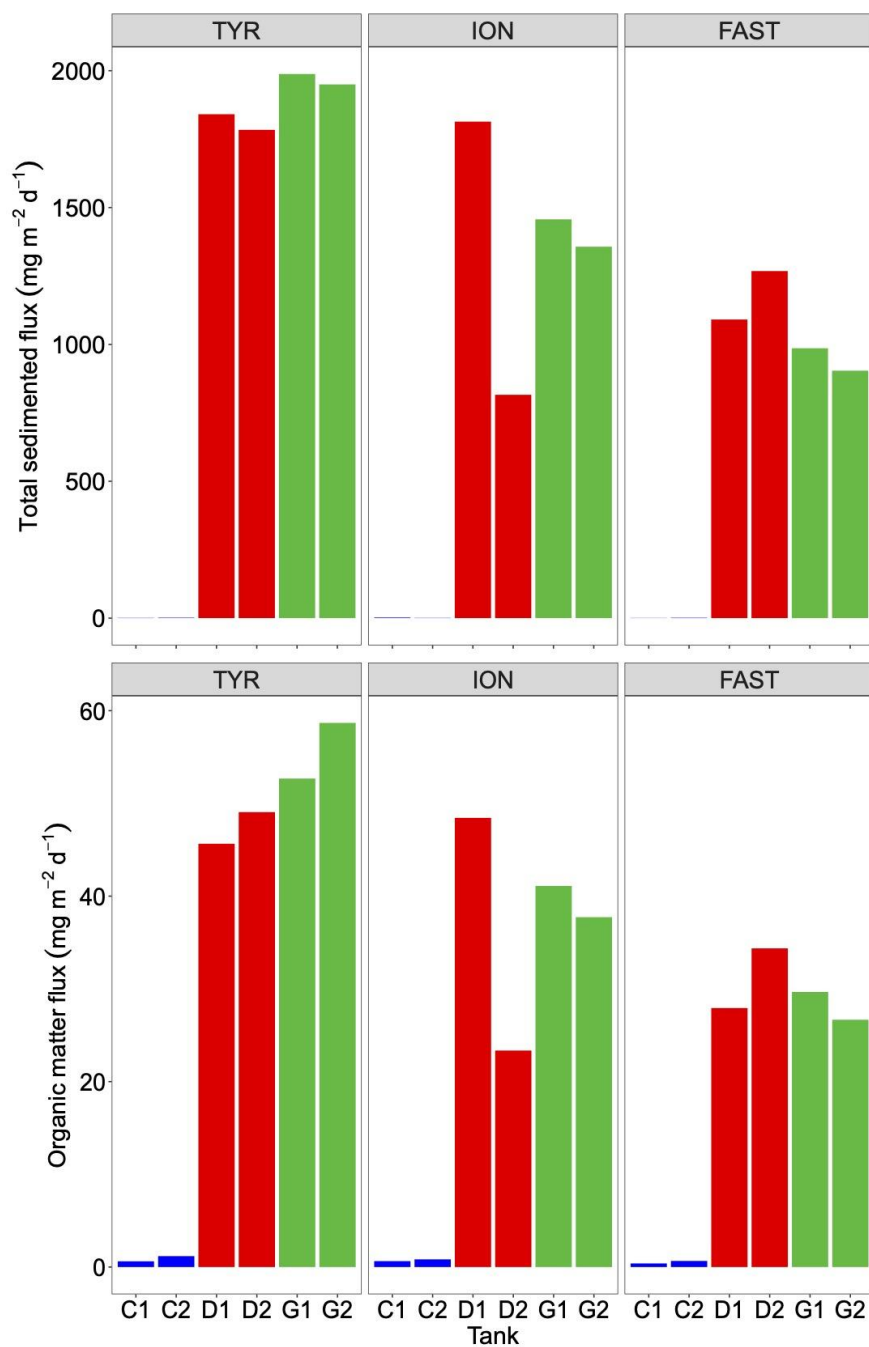
1327

1328 Fig. 6



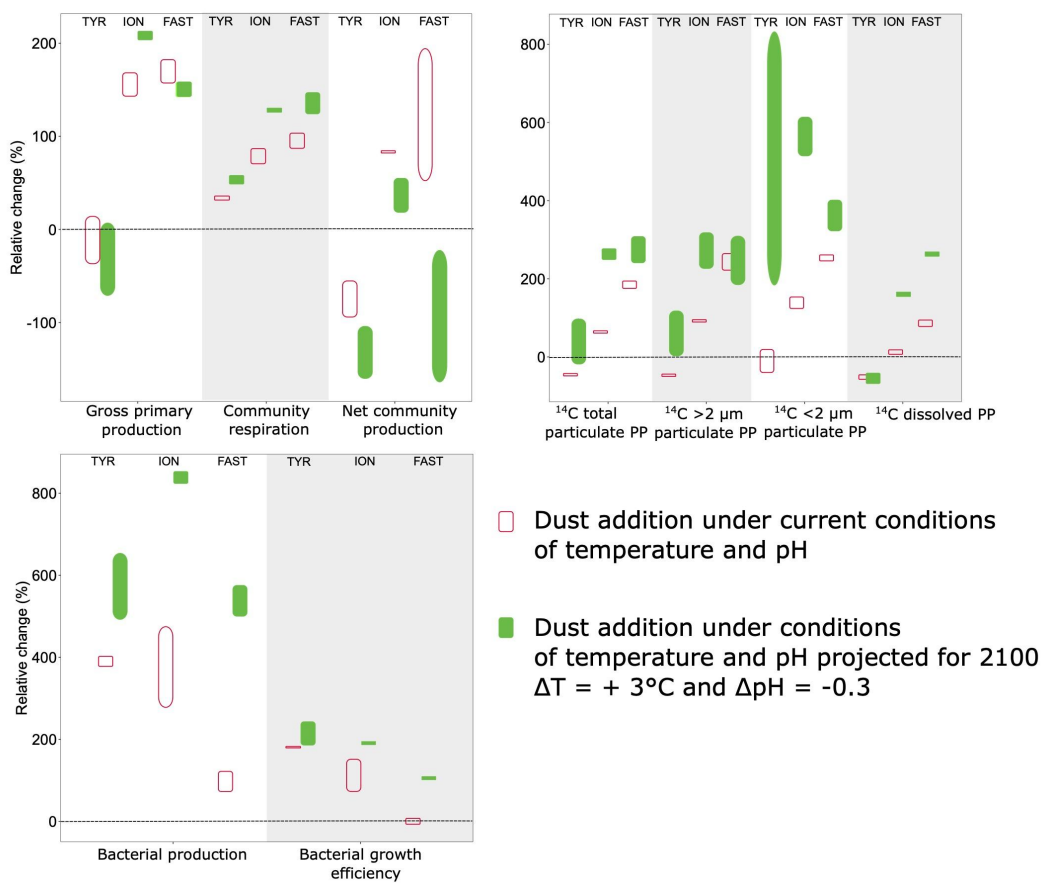
1329

1330 Fig. 7



1331

1332 Fig. 8



1333

1334 Fig. 9